ABSTRACT

GOODE, TYLER WAYNE. Soft Body Armor Back Face Deformation with Ballistics Gel Backing. (Under the direction of Dr. Mark Pankow).

Understanding how personal armor systems (PAS) deform during an impact event is paramount to their proper use in mitigating injury to the user. Most Kevlar® fabric characterization relies on testing fabric suspended in the air; however, in use, these materials may respond differently due to the resistance from the backing material. The current National Institute of Justice (NIJ) standard relies on a clay backing material, and measuring the deformation after impact. This does not provide any time dependent information about the deformation response of these materials.

In this work, a gas gun was used to fire projectiles into multi-layer Kevlar®-based PAS samples to characterize their protective responses. This experimental testing was performed using a backing material of clear ballistics gelatin that simulates the tissue of a human torso. The transparent characteristic of the gel allows multiple high-speed images of the back of the Kevlar® sample to be taken during the impact event. From these images, the maximum depth, width, and shape profile of the deformation can be tracked as a function of time.

Independent variables of impact energy, total areal density, fabric type, projectile type, and backing material stiffness were varied to examine their impact on the deformation response. Deformation depths were seen to increase with increasing impact energy and decreasing total areal density. PAS samples comprised of stiffer, thinner fabric saw slightly lower deformation depths than the thicker fabric PAS samples with the same total areal density. For example, it was observed that 122 g/m^2 Kevlar® KM2Plus fabric performs better per weight than 467 g/m^2 Kevlar® K29 fabric. Additionally, it was observed that 9mm full metal jacket (FMJ) projectiles produced deeper deformations than 12.7 mm steel ball bearings at the

same projectile energies. In addition to the projectile and sample variables, the ballistic gel stiffness also had a significant effect on the deformation response in both depth and shape.

Soft Body Armor Back Face Deformation with Ballistics Gel Backing

by
Tyler Wayne Goode

A thesis submitted to the Graduate Faculty of
North Carolina State University
in partial fulfillment of the
requirements for the Degree of
Master of Science

Mechanical Engineering

Raleigh, North Carolina

2017

APPROVED BY:

_____	_____
Dr. Scott Ferguson	Dr. Kara Peters

_____
Dr. Mark Pankow
Committee Chair

DEDICATION

I dedicate this thesis to my wife, Bonnie, who has patiently stood by my side through countless late nights, and has always encouraged me to be the best I can be.

BIOGRAPHY

Tyler completed his Bachelor of Science in Mechanical Engineering at the University of Alabama in the spring of 2015. In the fall of that year, he began a Master of Science in Mechanical Engineering at North Carolina State University, and began working in Dr. Mark Pankow's BLAST lab. In his second semester, Tyler began his research on ballistic fabrics and shape sensing for ballistic impacts under funding from the Department of Defense (DoD) Test Resource Management Center's (TRMC) Test and Evaluation / Science and Technology (T&E/S&T) Program. He was also awarded a fellowship from the National Science Foundation Graduate Research Fellowship Program (NSF GRFP) that he deferred for his Ph.D. study.

ACKNOWLEDGMENTS

I would like to thank my advisor Dr. Mark Pankow for his invaluable guidance while conducting this research, Dr. Scott Ferguson and Dr. Kara Peters for serving on my committee, Gary Lofton and Steve Cameron for fabricating test fixtures, and all the students in the BLAST Lab for their help with testing and ideas. I would also like to thank my family for always supporting me and believing in me.

This thesis research was completed under funding from the TRMC T&E/S&T Program, contracted through the U.S. Army Program Executive Office for Simulation, Training, and Instrumentation (Contract W900KK-15-C-0028), and while on reserve with an NSF Graduate Student Research Fellowship.

TABLE OF CONTENTS

LIST OF TABLES

LIST OF FIGURES

CHAPTER 1 - INTRODUCTION

This chapter will provide a background to ballistic fabric characterization and body armor testing techniques, as well as outline the objectives of this research.

1.1 – Background

Body armor has been used in various forms for centuries, and in the modern military age was normally made of cumbersome and bulky steel plates. Within the past few decades, advances in protective materials fostered a transition from steel plates to lighter ceramic plates. Unfortunately, parallel improvements in the lethality of small arms munitions developed a need for thicker ceramic plates, which offset their advantage in weight. These steel and ceramic approaches were primarily for military applications. However, in the 1970s, advances in high-strength polymer fibers enabled pure fabric armors (soft body armor) capable of stopping common threats. Armors using these high-strength fabrics were lighter weight and more flexible than previous armors, enabling everyday use even for non-military personnel. Since their introduction, much work has been done to characterize the performance of these high-strength fabrics, and evaluate the performance of personal protection systems that utilize them.

A ballistic fabric is composed of bundles of high strength fiber, called yarns, woven into a fabric that can have several different weave styles. Since plain weave fabrics exhibit the best performance [1], most armors and most research focuses on this style. A plain weave is the tightest weave and usually has roughly equal properties along its warp and weft directions (the two orthogonal weaving directions). For these fabrics undergoing ballistic impact, several energy dissipation mechanisms have been identified. Ha-Minh's modeling identified primary

energy dissipation mechanisms for armors: deformation of primary and secondary yarns, friction between yarns, friction between the yarns and projectile, and friction between fabric layers (for multiple layer samples) [2]. Because fabrics cannot transfer shear loads, yarns in line with the impacting projectile (primary yarns) take most of the load while adjacent yarns (secondary yarns) are only weakly loaded. Figure 1 shows how a fabric is loaded on impact with regions of primary and secondary yarn strain.

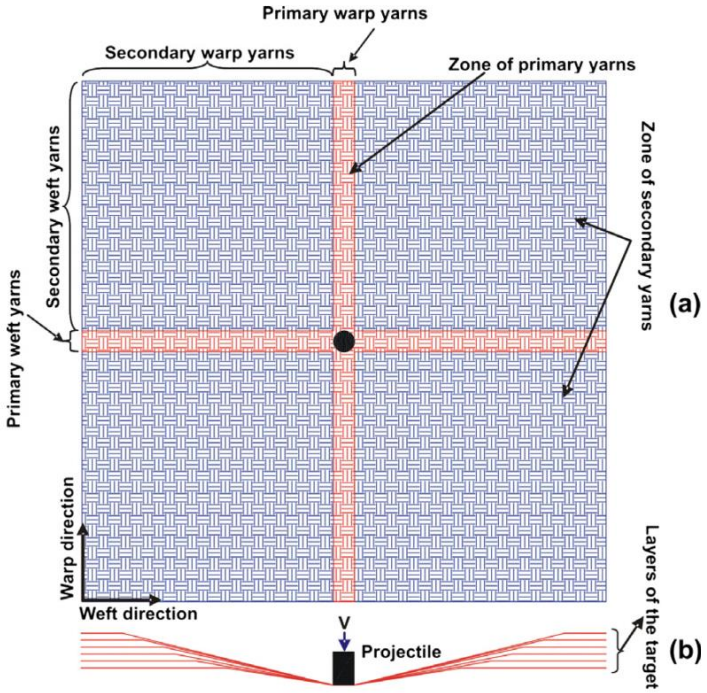

FIGURE 1. ZONES OF PRIMARY AND SECONDARY YARNS IN A FABRIC SUBJECTED TO IMPACT: (A) FACE VIEW AND (B) SIDE VIEW (FROM [2]).

This produces a pyramid shaped deformation that is seen consistently in fabric impacts. Figure 2 shows high-speed images of a fabric sample taken during a projectile impact.

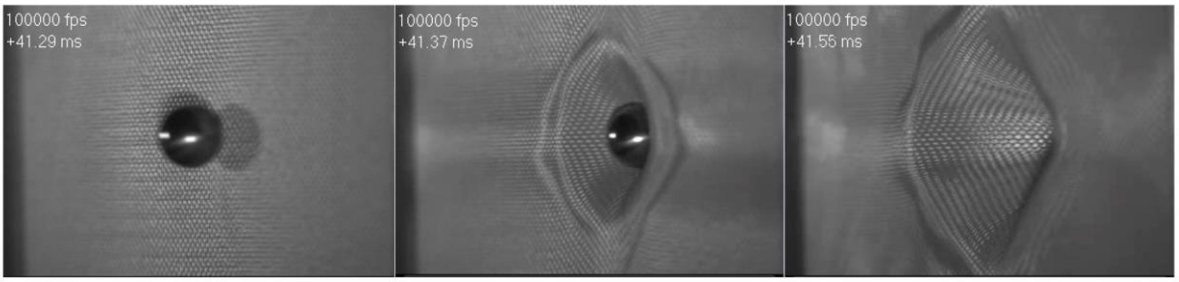

FIGURE 2. HIGH SPEED IMAGES FROM FRONT OF MULTIPLE LAYER FABRIC SAMPLE SHOWING DEVELOPMENT OF PYRAMID-SHAPED DEFORMATION.

As the projectile impacts the sample, the primary yarns can be seen loading (lighter color) and the deformation forms the pyramid shape expected for impact of a fabric.

The penetration and deformation behavior of ballistic fabrics is fairly well understood. Reviews by Cheeseman [3], Tabiei [4], Singh [5] and Sockalingam [6] summarize the majority of the work, and many of the mechanisms and influence parameters have been studied in detail [7]–[21]. While much progress has been made characterizing ballistic fabrics, little work has been done since the 1970s (when soft body armor was initially developed) to characterize back face deformation behavior of unclamped fabric samples supported by a tissue-simulating backing material. Since this is closest to how the fabrics are actually used in protection systems, it should be of primary importance. Body armors that enter service must undergo significant testing under these conditions, but only limited data is available due to the proprietary nature of the armor products. Since even a stopped projectile can produce serious injury [22], understanding the deformation behavior resulting from these events is also of paramount importance. This injury from a stopped projectile is called behind armor blunt trauma (BABT). BABT is a non-penetrating injury resulting from projectile impact, and occurs when the energy from the retarded bullet is deposited through the armor and into the wearer [23]. Cannon [24]

states that BABT is becoming a bigger problem as projectile energies from expected threats are increasing. To mitigate this worsening problem, understanding and predicting the back face deformation of body armor subjected to projectile impact, as well as understanding the dynamics of the event, is of paramount importance.

Body armors in use today are tested in accordance with the NIJ standard [25] to determine resistance to penetration and ensure that the maximum depth of the back face deformation does not exceed a fixed limit. However, the data obtained in this clay-backed ballistic testing is severely limited since only the residual plastic deformation of the backing material can be measured. No information is available of how the deformation propagates during impact. Although this is the standard test procedure, it is known that other factors influence the survivability of a projectile impact besides just the maximum deformation, such as the deformation rate and volume of deformation [23]. In addition, clay has been proven to show some elastic recovery [26] potentially making the measured maximum deformations incorrect.

The initial research that the NIJ standard is based on is a group of studies in the 1970s undertaken at the US Army Aberdeen Test Center that correlated back face deformations in various backing materials to injury probability in goats [27]–[33]. The authors decided to recommend the use of Roma Plastilina #1 modeling clay because it was cheap and readily available, and was a conservative analog to the goat as a backing material. The authors suggested that their technique was provisional, since not enough data was available to validate its accuracy [32]. However, the process has survived due to its practical success and relatively

low cost [23]. Figure 3 shows a plot of deformation behavior of various backing materials evaluated by Prather in the foundational study.

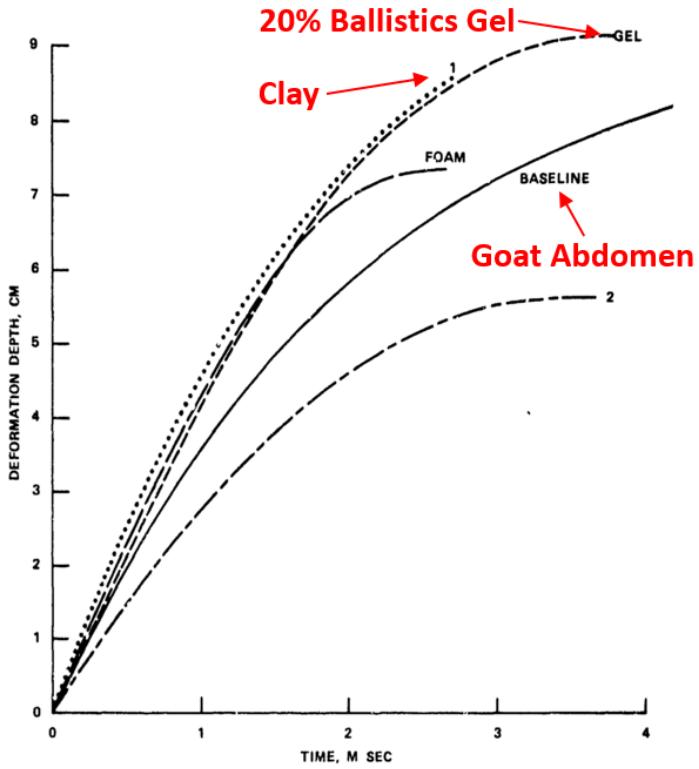

FIGURE 3. TIME DEFORMATION DATA OF VARIOUS BACKING MATERIALS [32].

The data in Figure 3 is from low speed impacts of a 200 g hemispherical projectile. Since they both recorded higher deformations than the baseline goat abdomen, both the FBI standard 20% ballistics gel and Roma Plastilina #1 clay were thought to be suitable materials providing conservative measurements. Clay was chosen because at the time, the high speed photography needed to record the deformation in ballistics gel was prohibitively expensive and difficult to use and implement [23]. However, since these materials exhibit high strain rate sensitivity

[34]–[36], it is questionable whether this correlation is applicable to the higher speed impacts seen from body armor back face deformation.

One major advantage of the ballistic gelatin is that a plethora of data can be obtained since the deformation can be imaged while the impact is in progress. The profile can be tracked as a function of time to determine how quickly the maximum depth is obtained, as well as how the shape of the deformation develops. High speed imaging has come a long way since the Prather study, and due to new, solid-state sensor technologies, high-speed cameras are no longer prohibitively expensive to operate [37]. Therefore, a recent study undertaken by the National Academies of Sciences, Engineering, and Medicine (NASEM) Board on Army Science and Technology (BAST) on how body armor testing should be improved recommended that ballistics gel be revisited as a backing material to use in future techniques [26]. In addition, new synthetic ballistic gelatins have much longer shelf lives than natural gelatins, and can be reused without showing degradation in mechanical properties. Figure 4 shows a block of clear synthetic gelatin available from Clear Ballistics™.

FIGURE 4. BLOCK OF SYNTHETIC BALLISTIC GELATIN AVAILABLE FROM CLEAR BALLISTICS™.

Ballistics gelatin is potentially a better analog to body tissue [38], and recent work has been done to characterize shockwave development and high rate properties that would enable measurement of forces and energies in the backing material [39]. Researchers have also placed pressure sensors in the gel, to determine the pressure wave magnitudes that develop from the impact [40]. Two types of ballistic gelatins are available, gel calibrated to the FBI standard (10% gelatin) and gel calibrated to the NATO standard (20% gelatin). The NATO standard gel is stiffer because they require a stiffer material to stop the full metal jacket (FMJ) projectiles used by NATO countries. Since there is interest in future testing with ballistics gelatin, it is desirable to be able to predict the behavior of high strength fabrics, such as Kevlar®, supported by these backing materials.

1.2 – Research Objectives

Objective 1: Develop a method of gathering time dependent data about body armor back face deformation during ballistic impacts.

Objective 2: Determine how parameters such as projectile velocity, total areal density, fabric layer thickness, projectile type, and backing material stiffness affect the deformation response of ballistics gel backed Kevlar® fabric specimens.

1.3 – Thesis Outline

Chapter 2 lays out the testing procedure developed to obtain data during ballistic testing with ballistics gel backing materials and provides details to the materials utilized in this work. Example codes for data processing are given in the Appendix A. Chapter 3 presents the results

of the ballistic testing, including how the various parameters studied affect the impact response of the body armor specimen. A table with the results from all test shots is given in Appendix B. In Chapter 4, some overall conclusions are drawn from this research, and recommended future work is discussed.

CHAPTER 2 – METHODS AND MATERIALS

A gas gun was used to fire projectiles at multi-layer Kevlar® samples of various compositions with a ballistics gel backing material. High-speed imaging was used to obtain video of the back-face deformation for each impact event. More detail is given in the following sections.

2.1 – Gas Gun

Figure 5 shows the gas gun used to simulate the body armor ballistic testing. The gas gun uses compressed helium to fire a projectile through the barrel and into the containment chamber. To release the compressed gas quickly enough to fire the projectile, a high flow rate, solenoid valve is used. The barrel used in this testing was a 2 m long, smoothbore, .50 caliber (12.7 mm in diameter). With this setup, .50 caliber (12.7 mm) projectiles can be fired directly, and anything smaller can be fired using a sabot. A sabot is a device that ensures the correct positioning of a bullet in the barrel of a gun when the diameter of the bullet is less than the diameter of the barrel, allowing the buildup of gas pressure behind the bullet, and falls away as the bullet leaves the muzzle. A single firing tank is used that can be pressurized up to 40 MPa. In this configuration, an 8 gram projectile can be fired at up to 600 m/s.

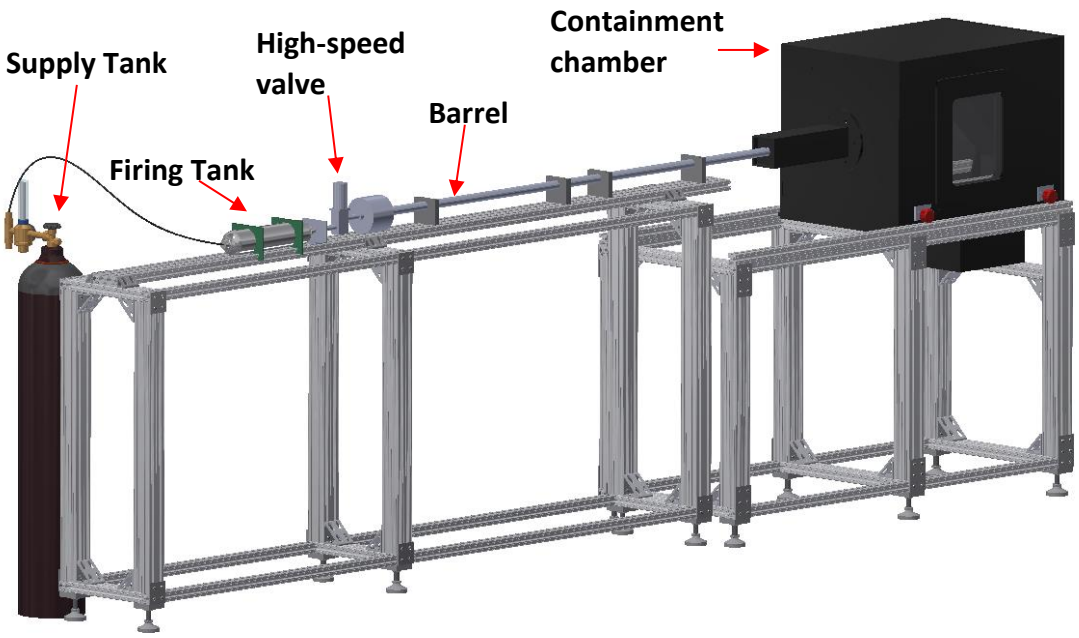

FIGURE 5. THE GAS GUN SYSTEM FOR PROJECTILE SIMULATION IN A CONTAINED ENVIRONMENT.

Two different projectiles were used in this work, 12.7 mm diameter steel ball bearings, and 9 mm FMJ rounds, which each have a mass of approximately 8 grams. The steel ball bearings were used for the majority of this testing due to their better consistency shot-to-shot than deformable projectiles, and ease of modeling for future work. Because the same 12.7 mm diameter barrel was used on the gas gun for both projectiles, sabots were needed to fire the 9 mm FMJ projectiles accurately. For this work, a sabot catch was not yet installed, resulting in the sabots also impacting the target, usually at the same time as the projectile. Since the sabot impacted with the projectile, the total mass of the projectile plus the sabot was used in calculating impact energies for the shots that utilized a sabot. A comparison of properties of the two projectiles is given in Table 1.

TABLE 1. COMPARISON OF IMPORTANT PROJECTILE PARAMETERS.

	9mm FMJ	*Ball Bearing*
Shape	Round-nosed bullet 	Sphere 
Diameter	9.0 mm	12.7 mm
Mass	8.035 g	8.238 g
Sabot Mass	0.716 g	N/A

Projectiles are accelerated in the gas gun using compressed air released by a high-speed electronic valve. The starting gas pressure can be adjusted to control the speed of the projectile. Prior to entering the main containment chamber, the projectile passes through two photogates to measure the velocity. Figure 6 shows a schematic of this setup.

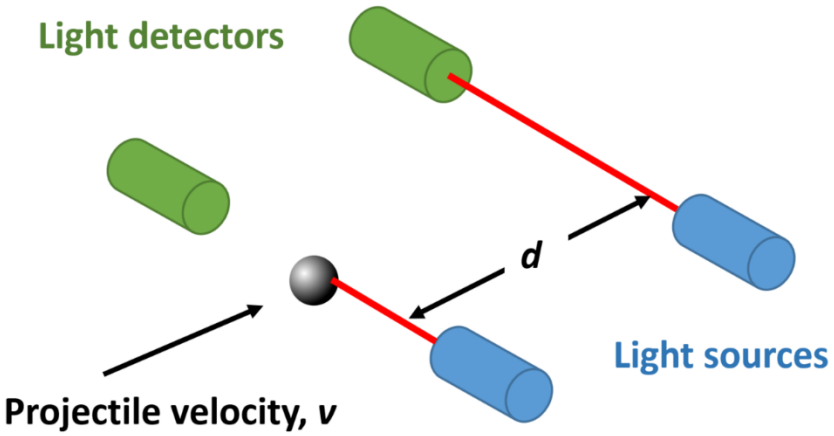

FIGURE 6. SCHEMATIC OF PHOTOGATE SETUP FOR MEASURING PROJECTILE VELOCITY.

The velocity of the projectile, v, is calculated using Eq. 1 where d is the distance between the photogates and Δt is the time between when the first and second photogates are tripped.

$$v = d/\Delta t \tag{1}$$

Figure 7 shows the containment chamber for the gas gun. The ballistics gel box is mounted in the containment chamber as shown in the figure. The containment chamber has a sliding metal enclosure providing access for sample mounting.

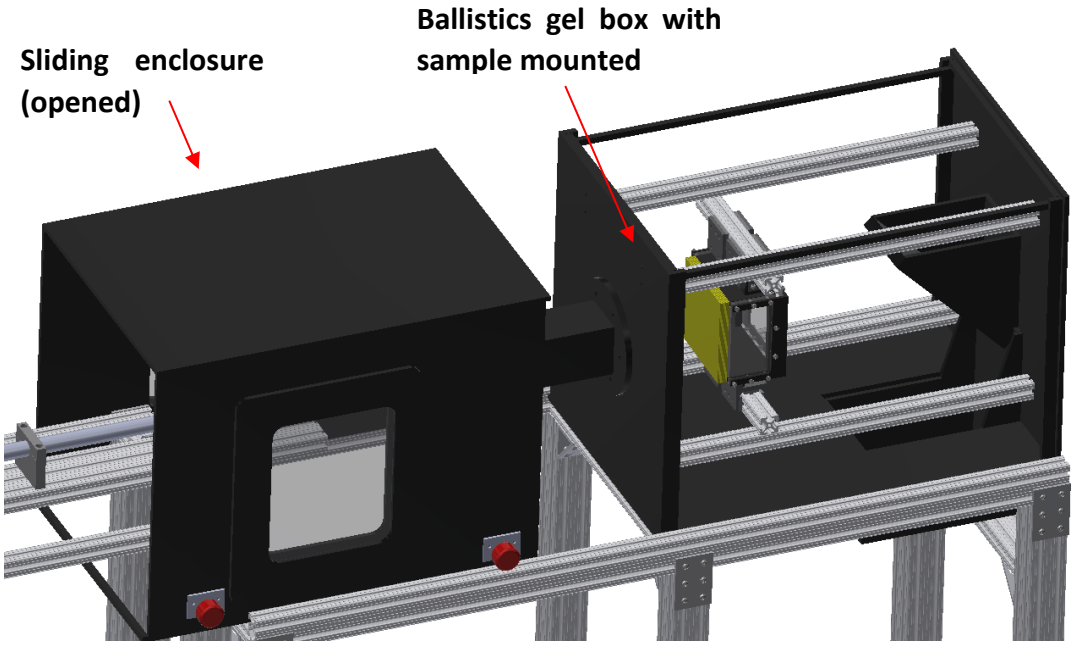

FIGURE 7. THE CONTAINMENT CHAMBER FOR THE GAS GUN WITH BALLISTICS GEL BOX AND SAMPLE MOUNTED INSIDE.

2.2 – Backing Material

Synthetic, completely transparent, ballistics gelatins made by Clear Ballistics™, were used as the backing materials for these tests. These synthetic gels are able to be remelted, allowing

them to be cast into our test apparatus. In this testing, it was observed that these gels can be reused numerous times without degredation in properties, providing consistent results shot to shot with little to no damage in the gel. NATO standard (20%) ballistics gelatin was used for the majority of the tests because of its stiffer response, with some tests conducted using FBI standard (10%) ballistics gelatin for comparison. Both gels experience significant strain rate sensitivity in their stress-strain response. Both stiffen considerably with increasing strain rate [35]. This strain stiffening would need to be considered when modelling the response of these materials under ballistic loading.

For testing with both types of gels, the ballistics gelatin was placed in a steel box with polycarbonate windows to allow for images to be taken of back face deformation during impact. The volume of gel inside the box measures 17.8 cm wide by 15.9 cm tall by 9.5 cm deep. The ballistics gel box is shown in Figure 8.

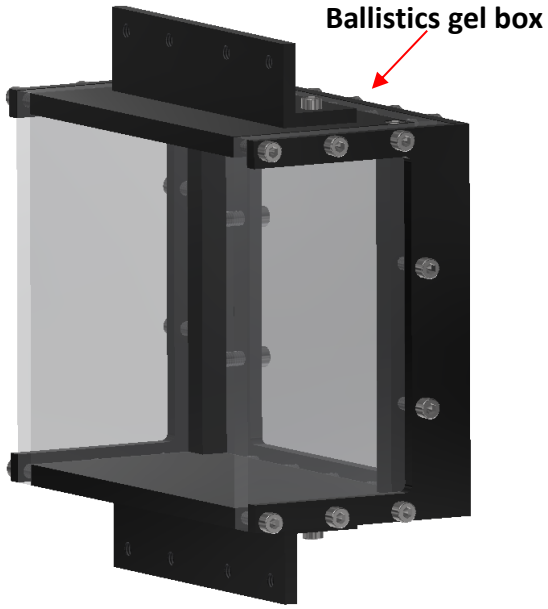

FIGURE 8. BALLISTICS GEL BOX.

2.3 – Ballistic Fabric Materials

Two Kevlar® fabrics were used in this testing. The properties of these fabrics are listed in Table 2. Kevlar® KM2Plus is slightly stiffer and stronger than the older K29. This does have a slight effect on comparability between the two fabrics.

TABLE 2. PROPERTIES OF THE TWO KEVLAR® FABRICS USED.

	Baseline (thick) Kevlar®	Thin Kevlar®
Yarn Material	Kevlar® K29	Kevlar® KM2Plus
Axial Modulus	70.5 GPa	72.4 GPa
Axial Strength	2.9 GPa	3.4 GPa
Yarn Thickness	3000 denier	500 denier
Weave	Plain	Plain
Areal Density	467 g/m^2	122 g/m^2
Warp/Weft Yarns	17x17 YPI	28x28 YPI
Treatment	Water Repellent	Water Repellent

Each sample was prepared to measure 16.5 by 16.5 cm, and consisted of multiple layers of fabric stacked together. Both plain-woven fabrics have equal properties in their respective 0° and 90° orientations (the fiber directions). The samples were prepared with the fiber directions aligned vertically and horizontally. Figure 9 shows examples of the multi-layer samples of each fabric with fiber orientation marked, while Figure 10 shows a close up of the weave with a ruler for scale reference.

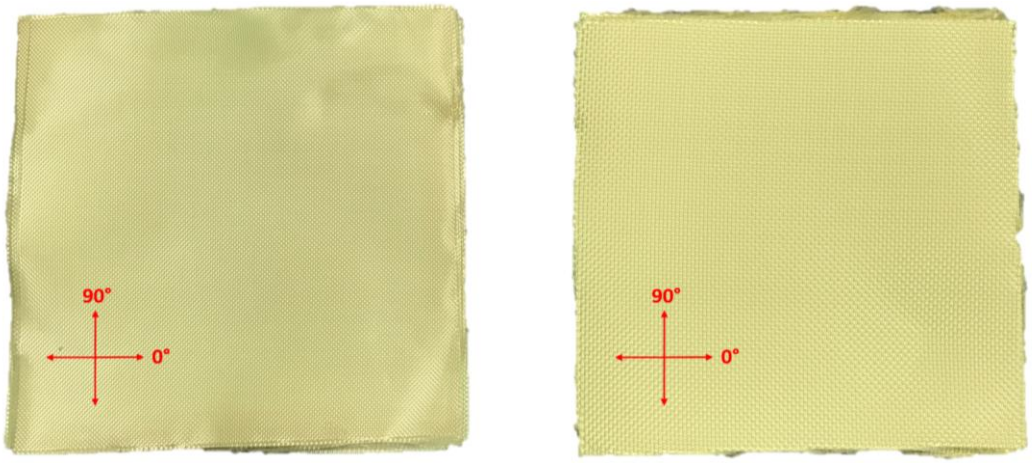

FIGURE 9. MULTI-LAYER SAMPLES OF THIN (LEFT) AND THICK (RIGHT) KEVLAR® FABRIC WITH FIBER ORIENTATION MARKED.

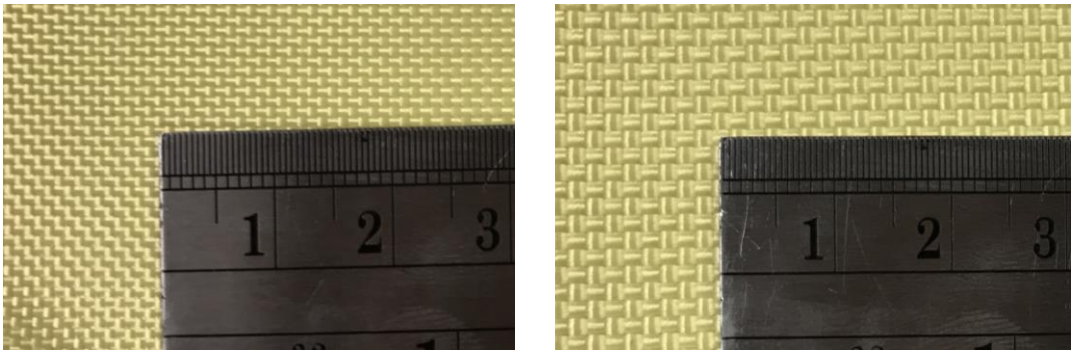

FIGURE 10. CLOSE UP OF THIN (LEFT) AND THICK (RIGHT) FABRICS TESTED IN THIS WORK (RULER DIVISIONS IN CM)

In commercial body armors, the ballistic fabrics are often stitched together to increase vest stability and to add another energy absorption mechanism. A 2008 study of stitching and layer effects in clay found a maximum 6.7% reduction in back face deformation depth for all the stitching patterns tested [41]. In this work, the multi-layer fabric samples were left unstitched for better consistency shot to shot. Samples are mounted on the ballistics gel box using vertical elastic straps spaced 9 cm apart, shown in Figure 11.

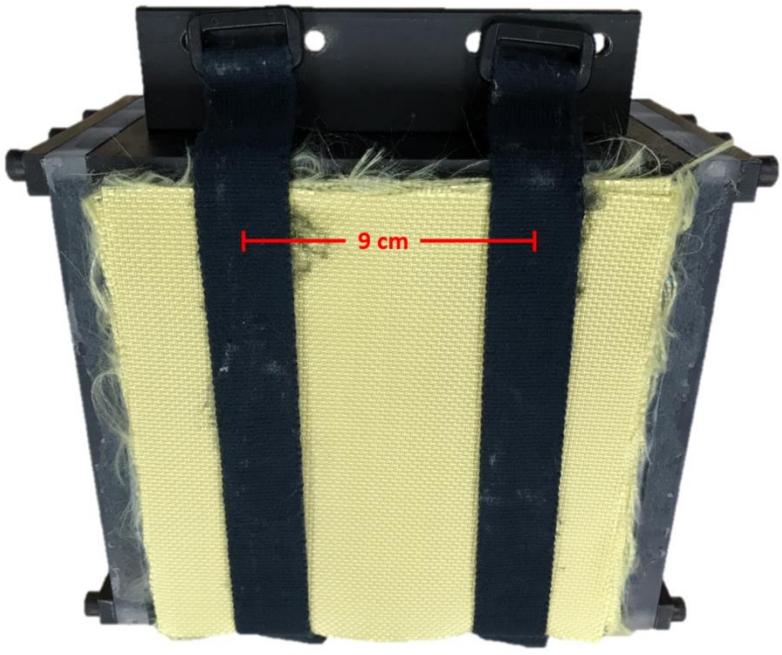

FIGURE 11. SAMPLE MOUNTED ON BALLISTICS GEL BOX USING ELASTIC STRAPS.

This mounting technique provides minimal effect on the response and allows quick turnaround between shots. The use of elastic straps in this manner is also consistent with the NIJ standard “acceptable strapping techniques” [25].

2.4 – High Speed Imaging

A Photron Fastcam SA-X2 (side) and a Photron Fastcam SA-Z (back) high-speed cameras were used to capture images of the impact event at 100,000 frames per second. One camera was placed with a side view of the deformation and one was placed with a back view. This allows for tracking the depth and shape of the deformation as a function of time. The side camera was set at a resolution of 384 by 264 pixels and rotated to capture the full deformations. This resolution gives a sensitivity of around three pixels per millimeter. The back camera was set at a resolution of 280 by 640 pixels giving a sensitivity of around five pixels per mm. This setup is shown in Figure 12 and Figure 13 (top view). Figure 14 shows a close up top view of the ballistics gel box in its testing configuration.

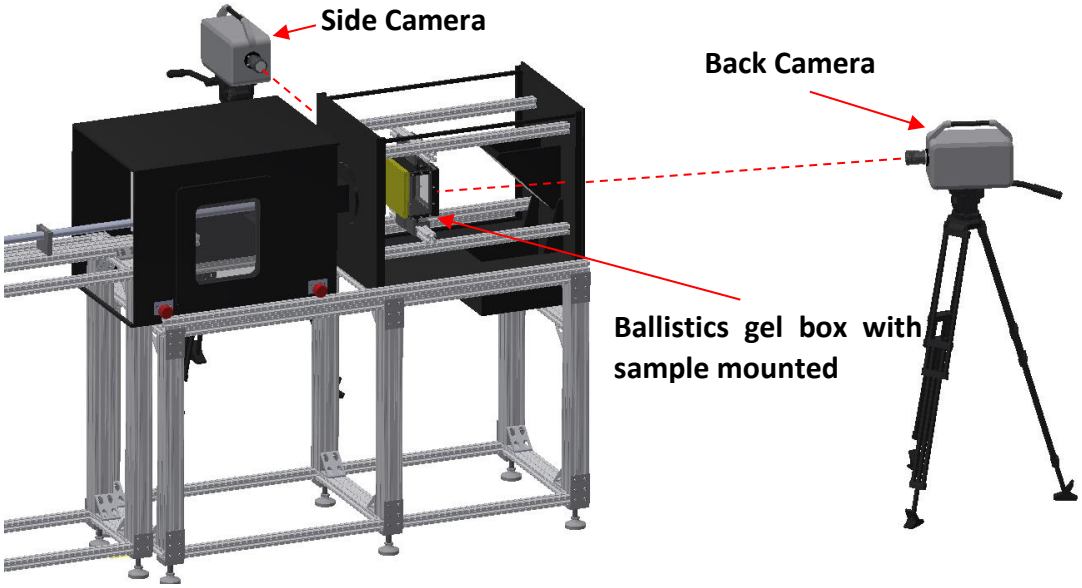

FIGURE 12. CAMERA LOCATION FOR GATHERING DEFORMATION SHAPE/DEPTH DATA.

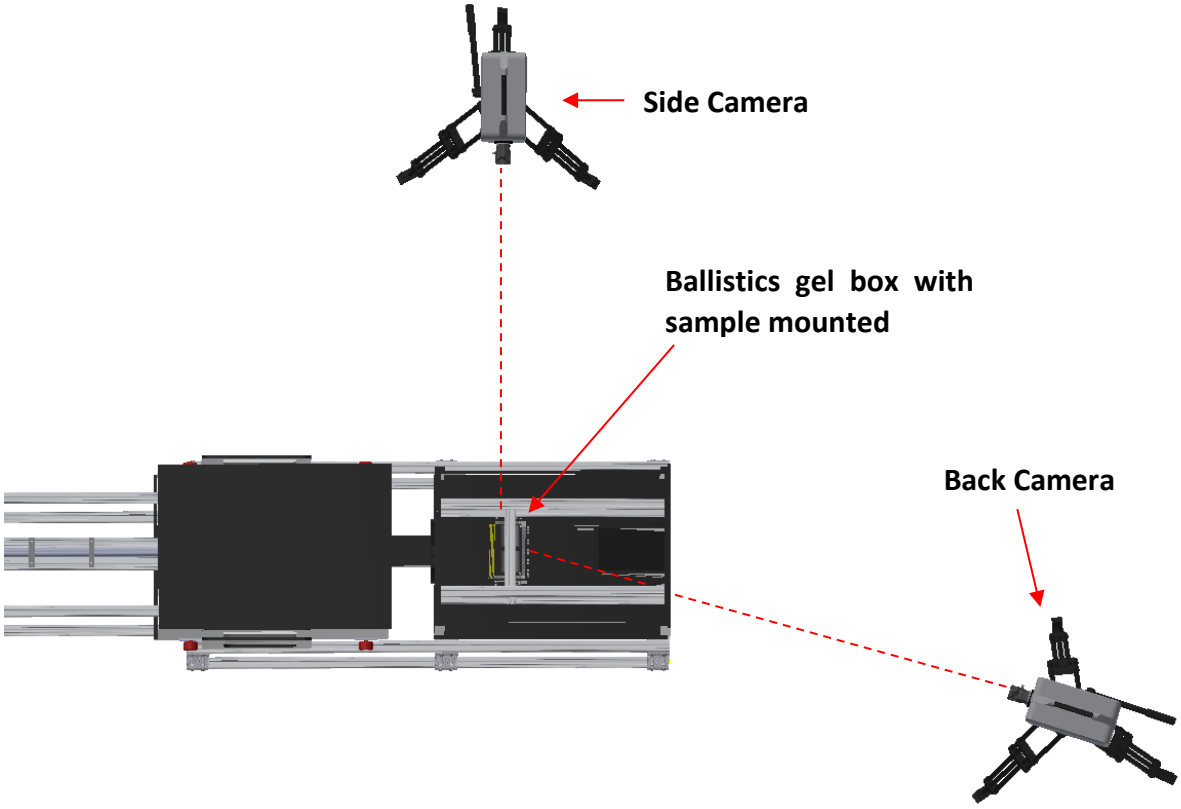

FIGURE 13. TOP VIEW OF CAMERA LOCATION FOR GATHERING DEFORMATION SHAPE/DEPTH DATA.

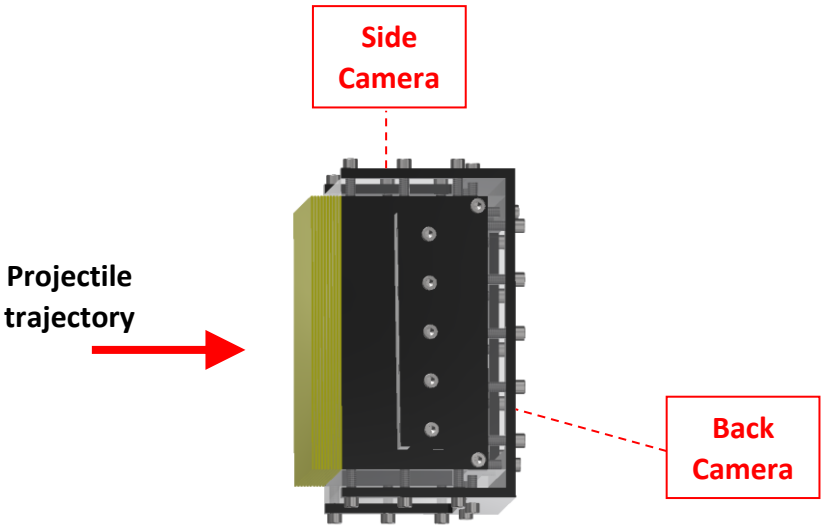

FIGURE 14. TOP VIEW OF BALLISTICS GEL BOX IN TESTING CONFIGURATION.

Example images from the side and back cameras are shown in Figure 15. From the side view, the side projected area and the depth of the deformation as a function of time can be calculated. The back view gives an idea of the cross-sectional shapes that are seen during testing.

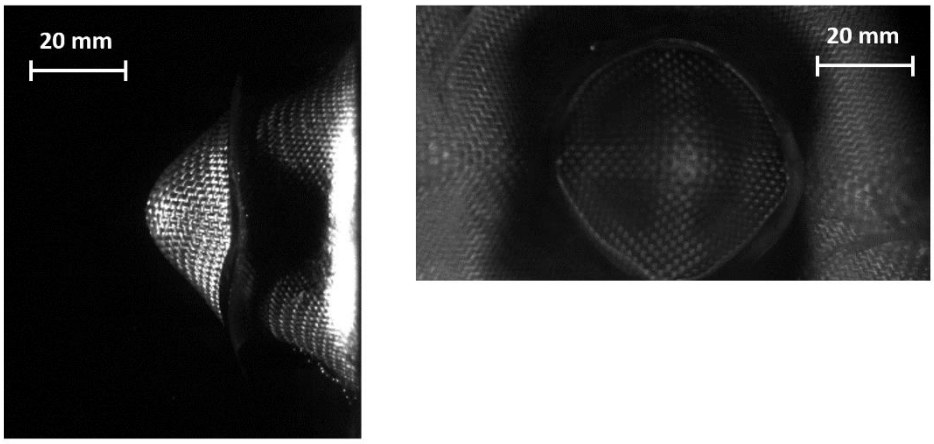

FIGURE 15. EXAMPLE IMAGES FROM SIDE CAMERA (LEFT) AND BACK CAMERA (RIGHT) DURING A PROJECTILE IMPACT.

Calibration images are taken with calibration rods of known depths pushed into the gel, prior to each round of testing. The calibration rods are shown in Figure 16.

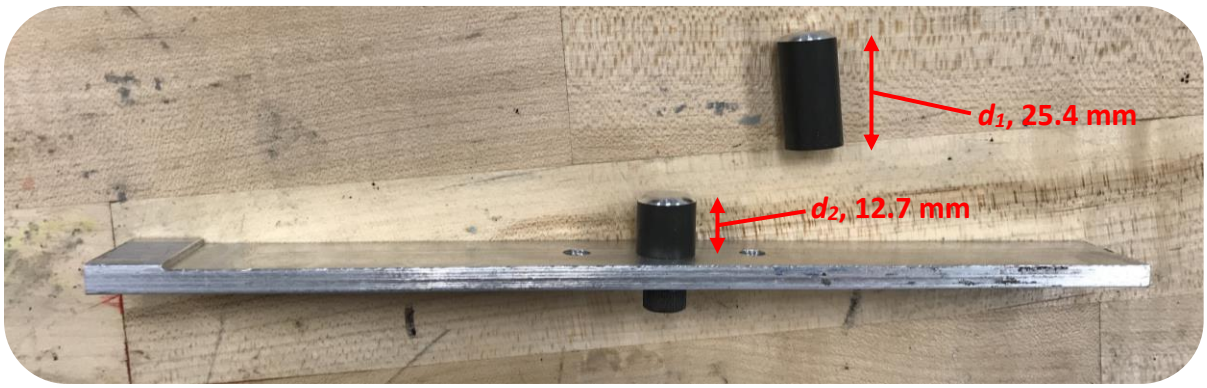

FIGURE 16. A 12.7 MM CALIBRATION ROD MOUNTED ON REFERENCE BAR AND 25.4 MM CALIBRATION ROD SHOWN UNMOUNTED.

At least two images with rods of different depths are needed to obtain a calibration. From the calibration images, the un-deformed material plane location is established as well as a calibration factor, *c*, in units of mm/pixel. Figure 17 shows typical calibration images taken in this work.

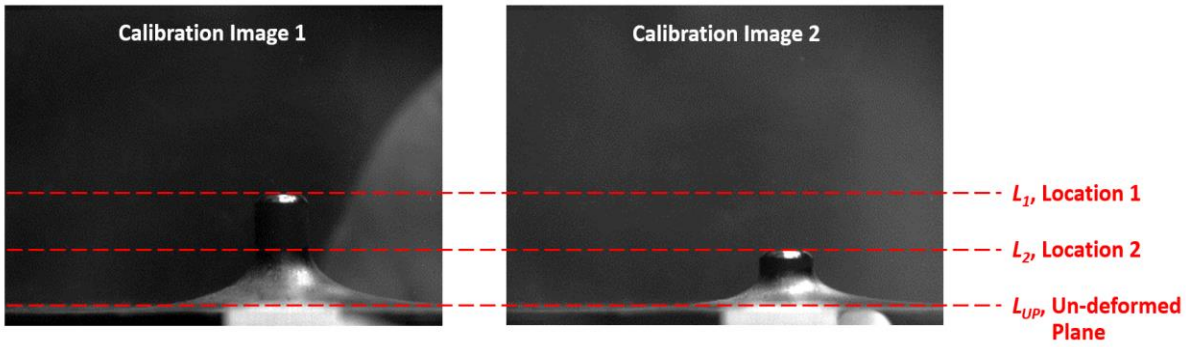

FIGURE 17. TYPICAL CALIBRATION IMAGES SEEN IN TESTING WITH IMPORTANT PIXEL LOCATIONS MARKED.

The calibration factor, *c*, can be calculated from Equation 2.

$$c = \frac{L_1 - L_2}{d_1 - d_2} \tag{2}$$

Where L_1 and L_2 are the pixel locations of the ends of the calibration rods in the depth direction, and d_1 and d_2 are the lengths of the calibration rods in millimeters. We choose d_2 to be half of d_1, and can then calculate the un-deformed plane location, L_{UP}, from Equation 3 using the locations L_1 and L_2.

$$L_{UP} = L_1 - 2(L_1 - L_2) \tag{3}$$

This provides a less subjective method for setting the location of the un-deformed material plane, L_{UP}. In the following section, it will be seen how these values are used to calculate depth, projected area, and volume of the observed deformations. It was assumed that the length

calibration in the depth direction was also valid for the width direction, since significant optical distortion was not observed in the images.

2.5 – Data Processing Method

This section describes the process of getting usable data out of the high-speed images. Edge detection was explored as a potential method for extracting data, but for the images obtained in this work, edge detection was unstable and it was difficult to back out the needed data. Therefore, an algorithm based on converting the images to black and white was used. First, the grayscale images from the camera are converted into binary images (black and white) where pixels in the deformation are white and pixels outside the deformation are black. Then, data such as maximum depth, width, projected area, and volume can be calculated using the black and white images The black and white conversion process used in this work is shown in Figures 18-22 for a 10 layer thick Kevlar® sample shot at 205 m/s.

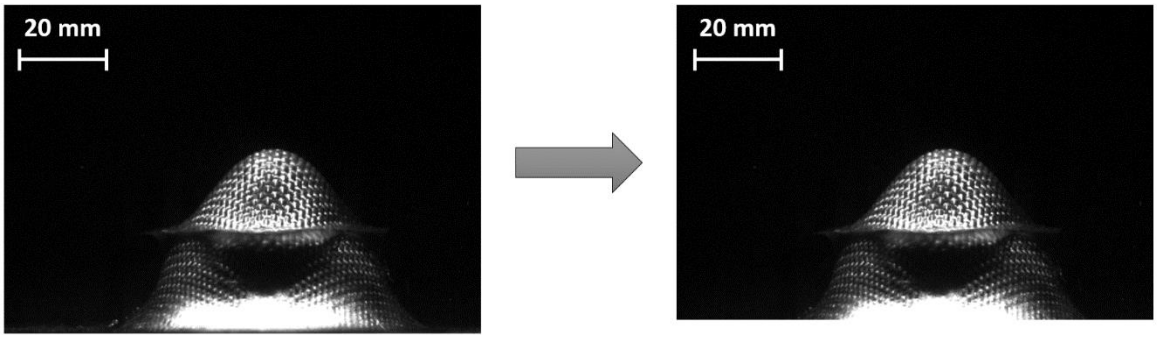

FIGURE 18. STEP ONE, CROP BOTTOM AT BASELINE (FROM CALIBRATION PROCEDURE)

Figure 18 shows how the raw image from the high-speed camera is cropped to the baseline location. This is done at the beginning so that the later code that calculates depths can be simpler.

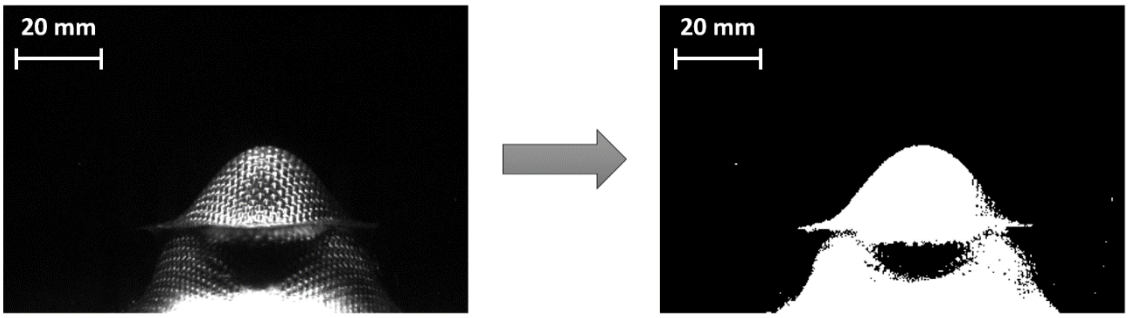

FIGURE 19. STEP TWO, CONVERT GRAYSCALE IMAGE TO BLACK AND WHITE.

Figure 19 shows the initial conversion to black and white. This was done using the "imbinarize" function in Matlab with a specified threshold. The threshold value that yielded the best results varied depending on shot and lighting conditions, but was typically between 0.02 and 0.12. Small artifacts from light reflected off impurities in the gel can be seen in the converted image.

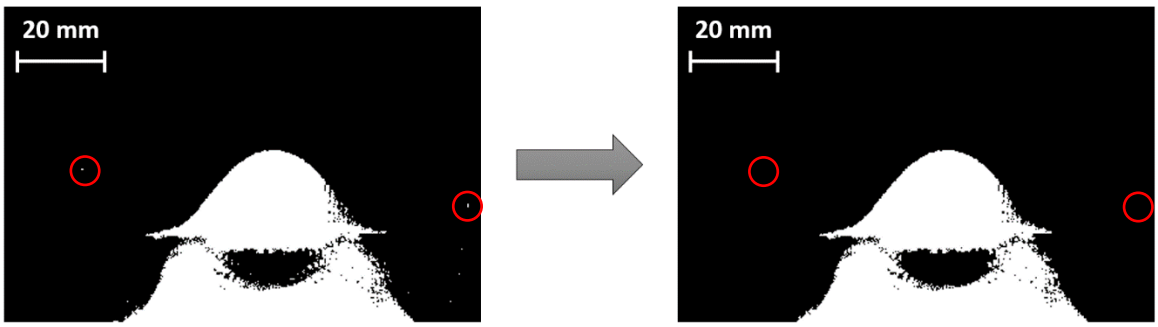

FIGURE 20. STEP THREE, DELETE ARTIFACTS IN IMAGE THAT ARE NOT PART OF THE DEFORMATION.

Figure 20 shows the deletion of the undesirable artifacts from the black and white image. This was done using the "bwareaopen" function in Matlab. The delete size for this function was typically around 20 pixels, but was increased for some tests to get rid of bigger artifacts.

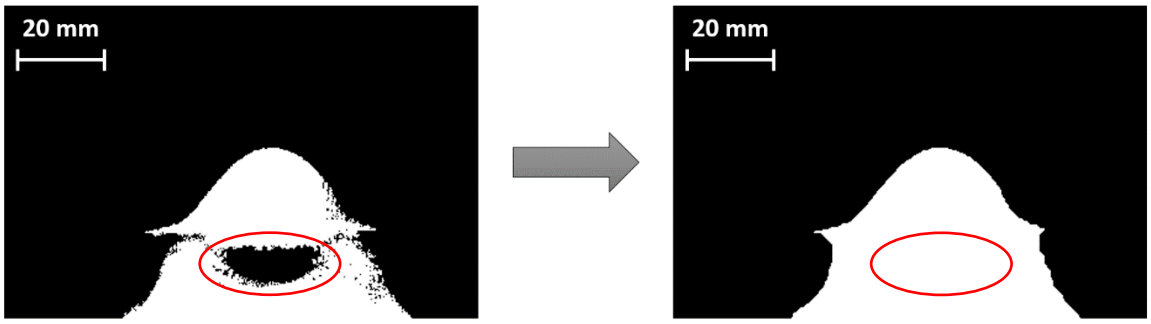

FIGURE 21. STEP FOUR, CLOSE GAPS IN THE DEFORMATION THAT RESULTED FROM DARK SPOTS IN THE IMAGE.

Figure 21 shows the black and white image before and after gaps in the deformation were closed. This was done so that the calculated projected area and volume values would accurately reflect the deformations. This was accomplished using the "imclose" and "imfill" functions in Matlab. The "imclose" function was used with a disk typically of size 15 pixels, but was increased for some shots which had bigger gaps in the detected deformation.

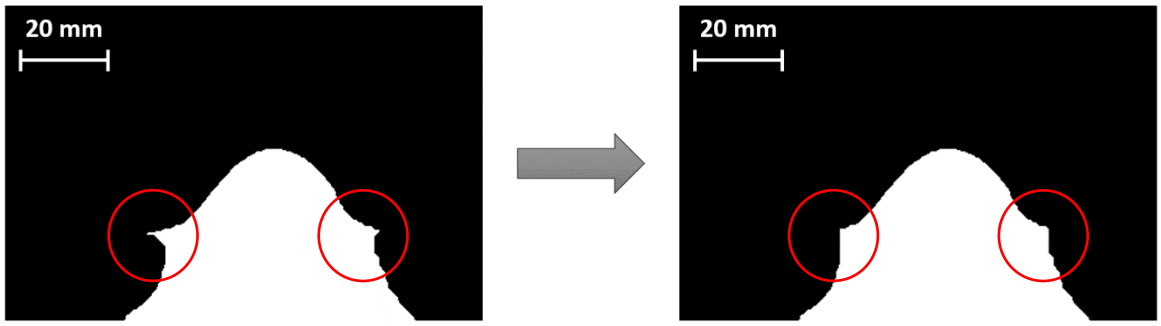

FIGURE 22. STEP FIVE, OPTIONALLY DELETE TRAPPED AIR RINGS TO IMPROVE CALCULATED VOLUME ACCURACY.

In shots above about 100 m/s, a ring of trapped air forms around the deformation and shows up in the images. Since this trapped air is not a part of the deformation, the associated pixels were removed from the data to more accurately reflect the projected area and volume of the deformations. Figure 22 shows an example of a black and white image before and after these

rings were deleted. Figure 23 shows the difference in the calculated volume when the rings are deleted versus being included for the same 10 layer, thick Kevlar®, sample shot at 205 m/s used for the previous figures.

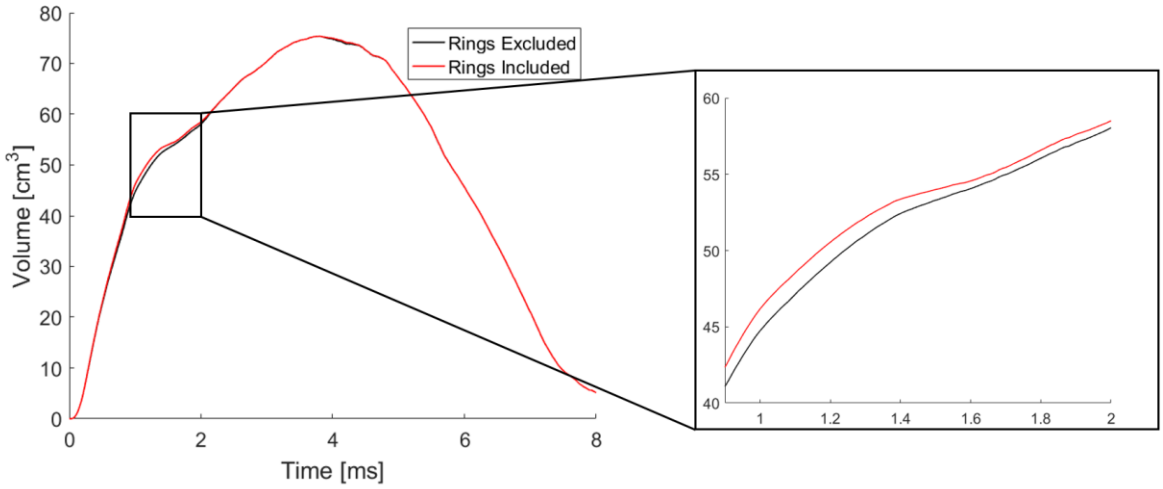

FIGURE 23. COMPARISON OF CALCULATED VOLUMES WITH AND WITHOUT INCLUDING TRAPPED AIR RING.

The volumes for each case are the same except in the region where the trapped air ring is present, which is highlighted. In this region, the maximum difference in calculated volumes is 1.45 cm^3 or 3.22% greater, when the air ring is included for this example. The image conversion process outlined in Figures 18-22 is implemented in the "convertToBW.m" example Matlab script given in Appendix A.

Once the black and white image data is obtained, parameters relevant to the testing can be obtained. The maximum depth and projected area are straightforward to calculate from the black and white images. The maximum depth is calculated by finding the difference between the deepest point of the deformation and the un-deformed plane location. The projected area, in square pixels, is just the quantity of white pixels in the black and white image. These

computed values, in pixels or square pixels, can be converted into physically meaningful units with the calibration factor discussed in the previous section. Figure 24 shows these parameters marked on an example black and white image.

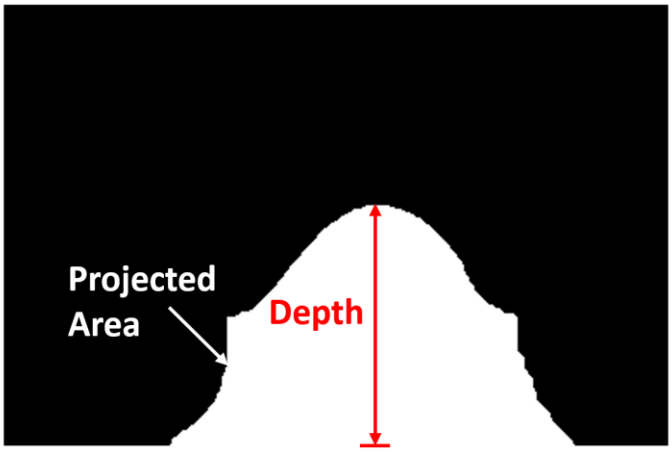

FIGURE 24. DEPTH AND PROJECTED AREA SHOWN ON AN EXAMPLE BLACK AND WHITE IMAGE.

Volume is slightly less trivial to calculate. First, assume that cross sections in the armor plane are circular (this assumption will be justified later). Then, volume can be calculated by revolving the area about the centroid axis parallel to the projectile. For example, given n pixels in the left side of the deformation, the volume predicted from the left side, V_{left}, is given by Equation 4 in cubic pixels. This is converted to physically meaningful units using the calibration factor.

$$V_{left} = \sum^{n} \pi \left[\left(r_i + \frac{1}{2} \right)^2 - \left(r_i - \frac{1}{2} \right)^2 \right] \tag{4}$$

Where r_i is the distance each pixel in the left side of the deformation is from centerline. For accuracy, the volume that follows from the right side of the deformation, V_{right}, is also calculated and the reported volume is the average of these values. The Matlab helper function

"findVolume.m" used to calculate the volume at each frame is given in Appendix A. Figure 25 shows a visualization of the volume an arbitrary pixel represents.

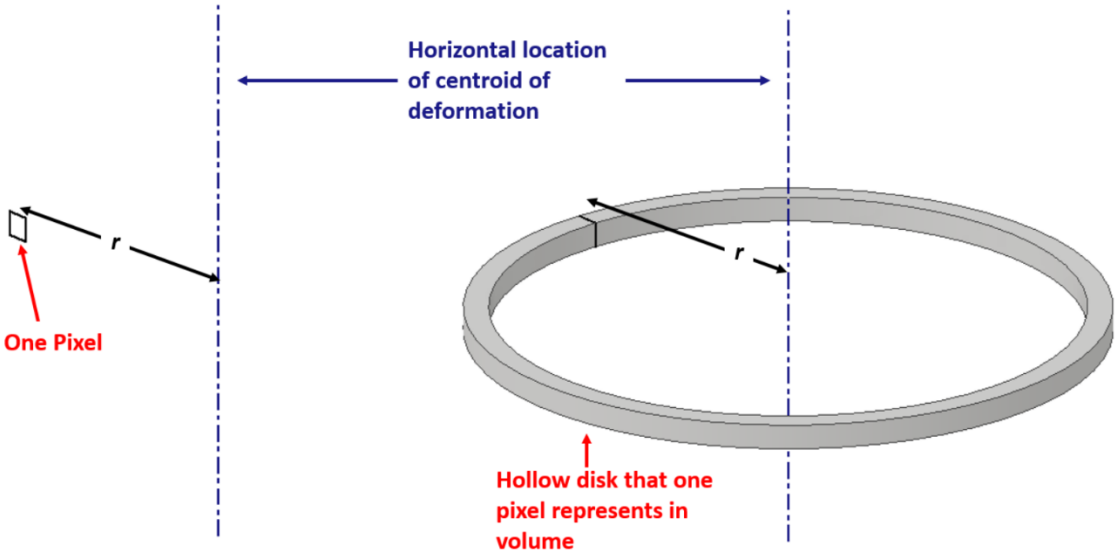

FIGURE 25. VISUALIZATION OF THE VOLUME OF AN ARBITRARY PIXEL.

The assumption of armor-plane circular cross-sections comes from observations of deformation shapes seen in testing. Figure 26 shows a snapshot of a deformation from the back and side camera views with the long and short dimensions of the rounded diamond shaped deformation marked.

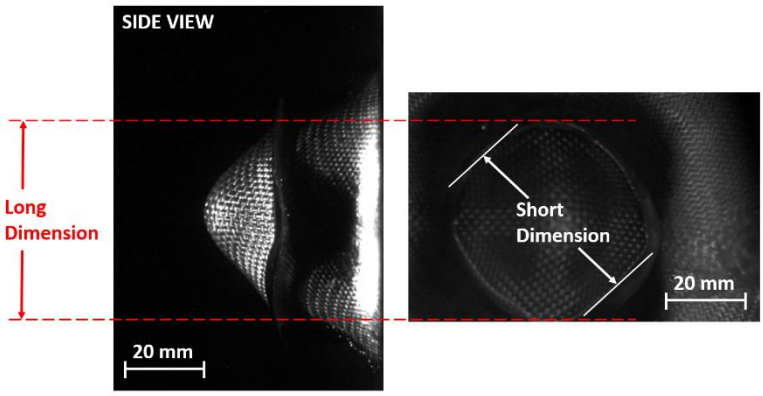

FIGURE 26. SNAPSHOT OF DEFORMATION FROM BACK AND SIDE VIEWS SHOWING LONG AND SHORT DIMENSIONS OF DEFORMATION.

It can be seen that a rounded diamond shape develops and the long dimension of the diamond is what is projected to the side camera. Therefore, the long dimension of the rounded diamond is what is measured by the camera, and what is used as the diameter for the idealized circular cross section. Figure 27 shows the idealized cross-section (red) overlaid on an actual cross-section (black).

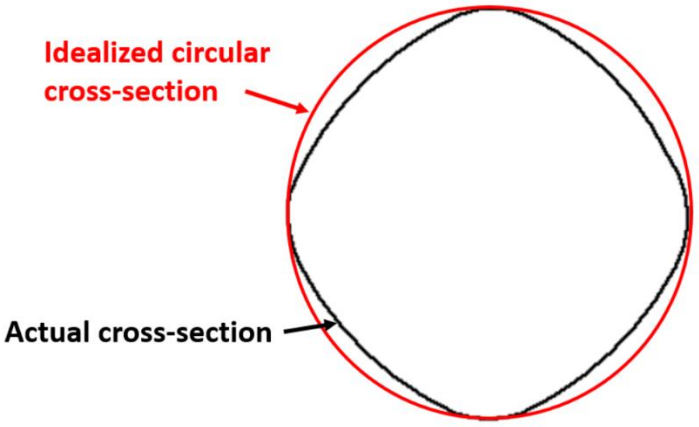

FIGURE 27. EXAMPLE IDEALIZED VERSUS ACTUAL ARMOR-PLANE CROSS-SECTION.

The idealized (circular) cross-sectional area is around 10% larger than the actual, meaning the calculated idealized deformation volume will be around 10% greater than the actual

deformation volume. For predictions of injury based on deformation volumes, these values will be conservative, since greater deformation volumes produce greater injury.

An example Matlab script called “writeData.m” is given in Appendix A that can be used to calculate the parameters discussed for a given shot.

2.6 – Conclusions

In this chapter, the testing setup and procedure used in this research is described. A technique for determining important time-dependent back-face deformation data is presented in detail, and assumptions for the deformation volume calculations are explained.

CHAPTER 3 – RESULTS

For each test, time dependent data was obtained for the deformation depth, side projected area, and volume. Since the side projected area is not as physically meaningful as the volume and is a similar parameter, only the volumes are presented.

3.1 – Baseline

Baseline tests were conducted using the 20% ballistics gel, thick fabric, and ball bearing projectiles. In later sections, various parameters will be varied and results compared to the baseline. Table 3 shows the baseline test parameters.

TABLE 3. PARAMETERS FOR BASELINE TESTS.

Fabric Type	thick
Number of Fabric Layers	5, 10, 15
Total Areal Density	2335-7005 g/m^2
Projectile	ball bearing
Projectile Velocity	50-350 m/s
Backing Material	20% Gel

An example of the time-dependent data for the baseline tests is given in Figure 28 of a test containing 10 layers shot at 205 m/s.

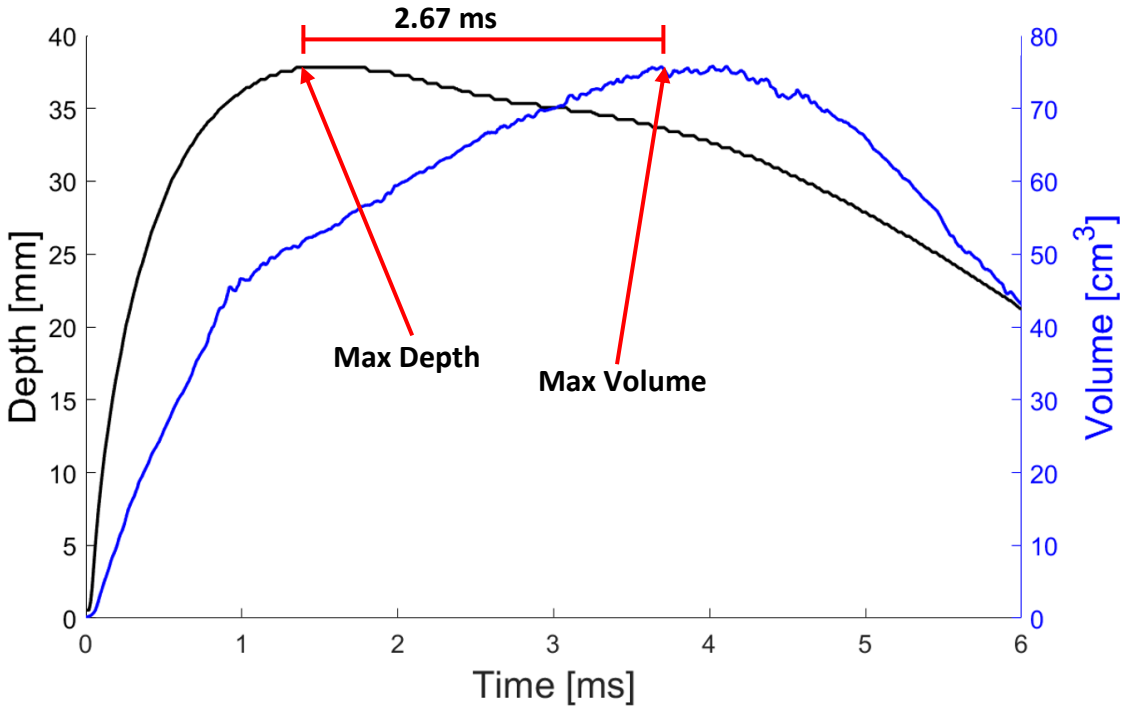

FIGURE 28. EXAMPLE OF DEFORMATION PARAMETERS AS A FUNCTION OF TIME AFTER PROJECTILE IMPACT FOR A 205 M/S IMPACT OF A BALL BEARING INTO 10 LAYERS OF THE BASELINE (THICK) FABRIC.

From these curves, the maximum deformation depth and volume, as well as the time to attain these values can be calculated. One thing that is interesting to note is that even after the deformation attains its maximum depth, the volume continues to increase. This is because the deformation continues to widen after the maximum depth is obtained. In the example test in Figure 28, maximum volume is not attained until 2.67 ms after the maximum depth is reached. This is critical data when trying to model trauma in the body from a projectile impact, since the initial deformation occurs over a much smaller area than a final deformation from clay testing would suggest. Figure 29 shows the evolution of the deformation profiles after maximum deformation for the example baseline test from Figure 28.

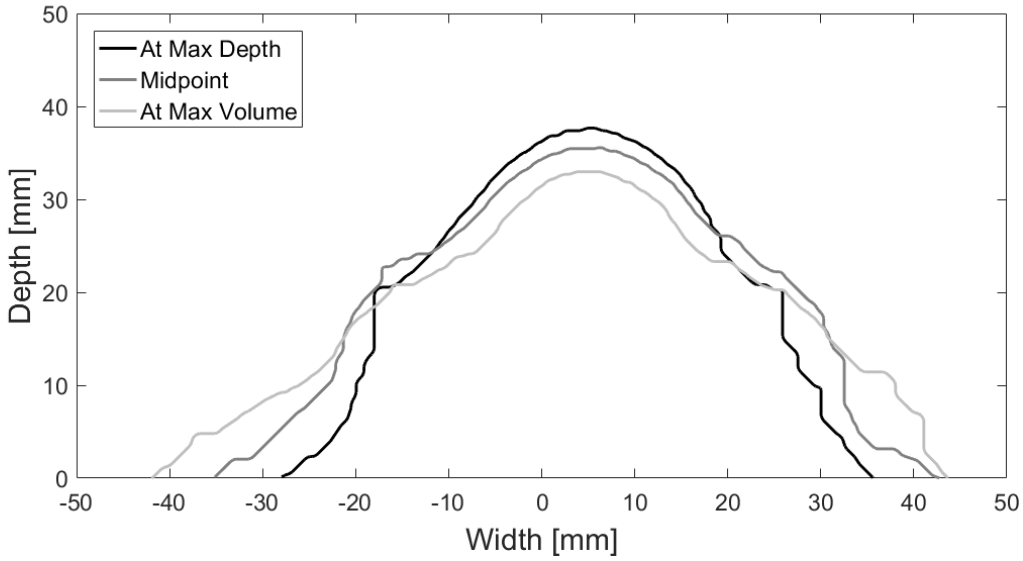

FIGURE 29. EVOLUTION OF DEFORMATION PROFILES AFTER MAXIMUM DEFORMATION IS REACHED.

It can be seen that after maximum depth is achieved, even though the depth is decreasing, the volume continues to increase as the deformation width continues to increase. Figure 30 shows a comparison of the maximum depths of all of the baseline tests.

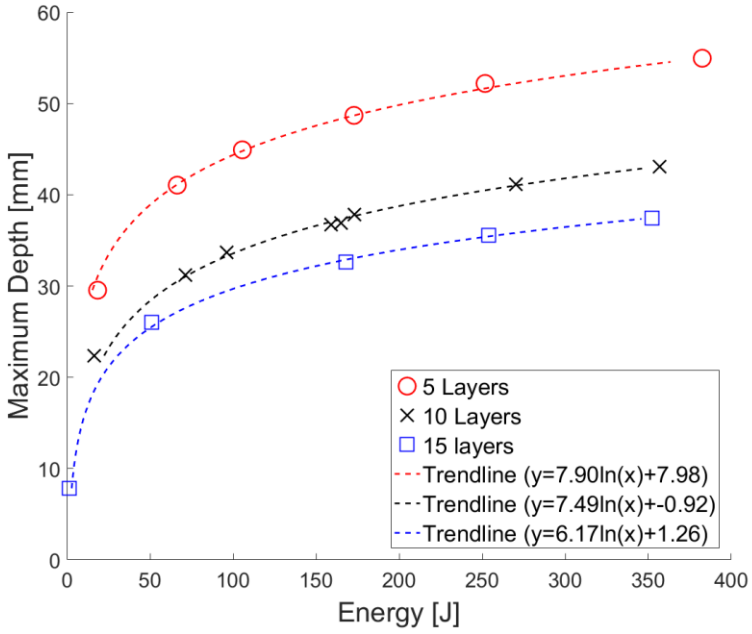

FIGURE 30. MAXIMUM DEPTHS SEEN IN BASELINE TESTING.

The maximum depths correlate positively with the projectile energy and negatively with the areal density (number of layers). This makes sense in light of known energy dissipation mechanisms. Having more material means more energy is able to be dissipated by material strain, yarn-to-yarn friction, and layer-to-layer friction on impact. Figure 31 shows the maximum volumes seen in baseline testing.

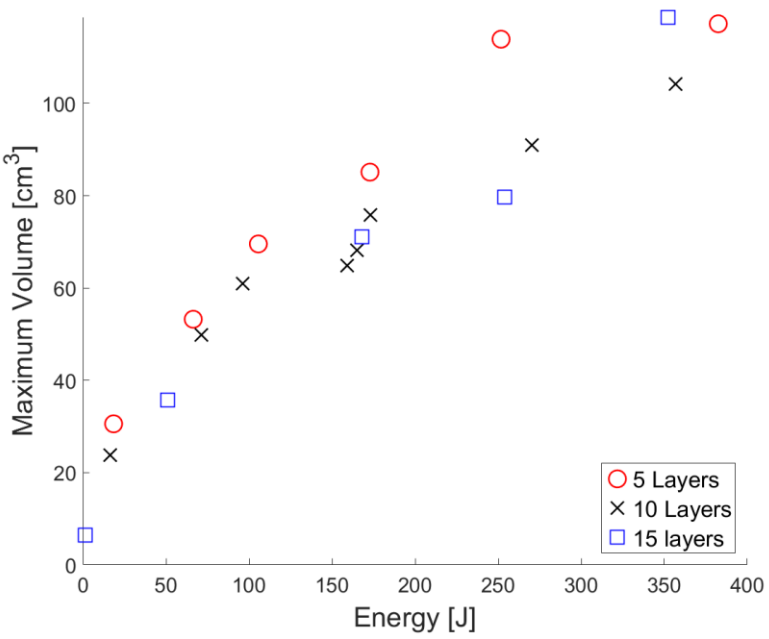

FIGURE 31. MAXIMUM DEFORMATION VOLUMES SEEN IN BASELINE TESTING.

The maximum volume correlates positively with projectile energy and negatively with number of layers, also. It appears that the maximum deformation volume is linearly correlated with the energy input into the system buy the projectile. This will be seen in later tests as well. The next sections show the effect of changing various test parameters on the maximum deformation depths, volumes, and shapes.

3.2 – Layer/Density Effects

Nine tests were conducted at a constant velocity of 200 ± 6 m/s to compare shapes and depths of deformations as the total areal density of the sample is increased. This was done with the same fabric so the only thing changing between tests is the number of layers in the sample, and consequently the total areal density. Table 4 shows parameters for this group of tests.

TABLE 4. PARAMETERS FOR CONSTANT VELOCITY LAYER COMPARISON TESTS.

Fabric Type	thick
Number of Fabric Layers	4-20
Total Areal Density	1868-9340 g/m^2
Projectile	ball bearing
Projectile Velocity	200 ± 6 m/s
Backing Material	20% Gel

Figure 32 shows how the shapes vary as more layers are added.

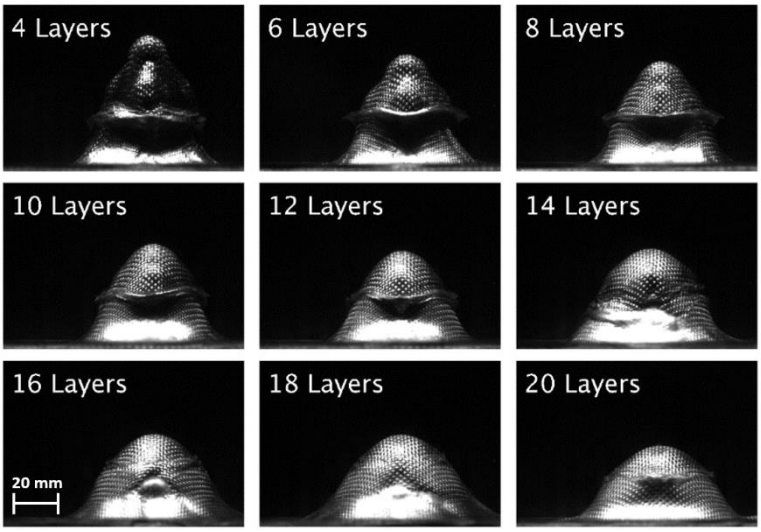

FIGURE 32. DEFORMATION PROFILES FOR CONSTANT VELOCITY TESTING AT POINT OF MAXIMUM DEFORMATION DEPTH.

Predictably, the deformation profiles become shallower as the areal density of the sample is increased. Figure 33 shows a cascade plot of the deformation profiles of these tests for more direct depth and shape comparison.

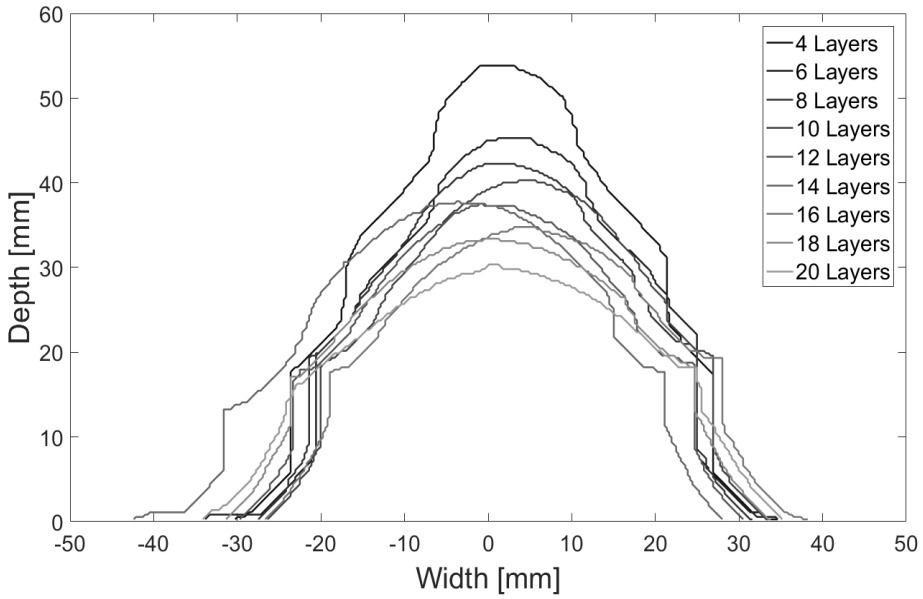

FIGURE 33. PLOT OF SHAPES FROM CONSTANT VELOCITY TESTING AT POINT OF MAXIMUM DEPTH.

The deformation profiles become rounder and less pointed as the total areal density increases (represented by number of layers), while the maximum depths predictably decrease. In addition, it can be seen that the widths of the deformations stay relatively constant. Figure 34 shows the profiles at the point of maximum volume.

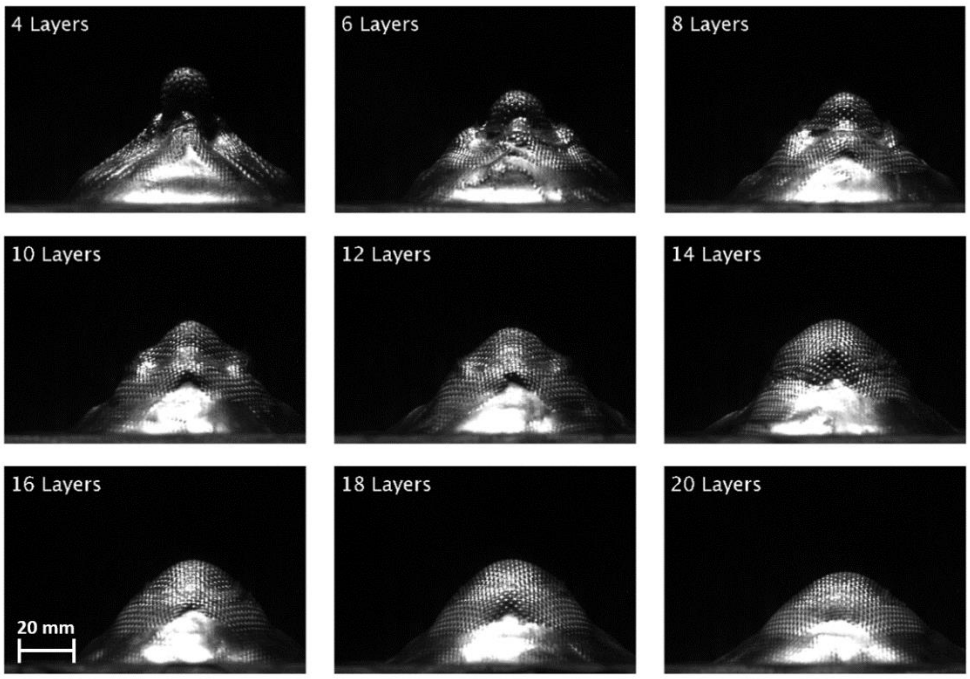

FIGURE 34. DEFORMATION PROFILES FOR CONSTANT VELOCITY TESTING AT POINT OF MAXIMUM DEFORMATION VOLUME.

After the deformation reaches its maximum depth, the deformation continues to widen and increase in volume, while remaining near the maximum depth. Figure 35 shows a cascade plot of the profiles of the deformations from Figure 34.

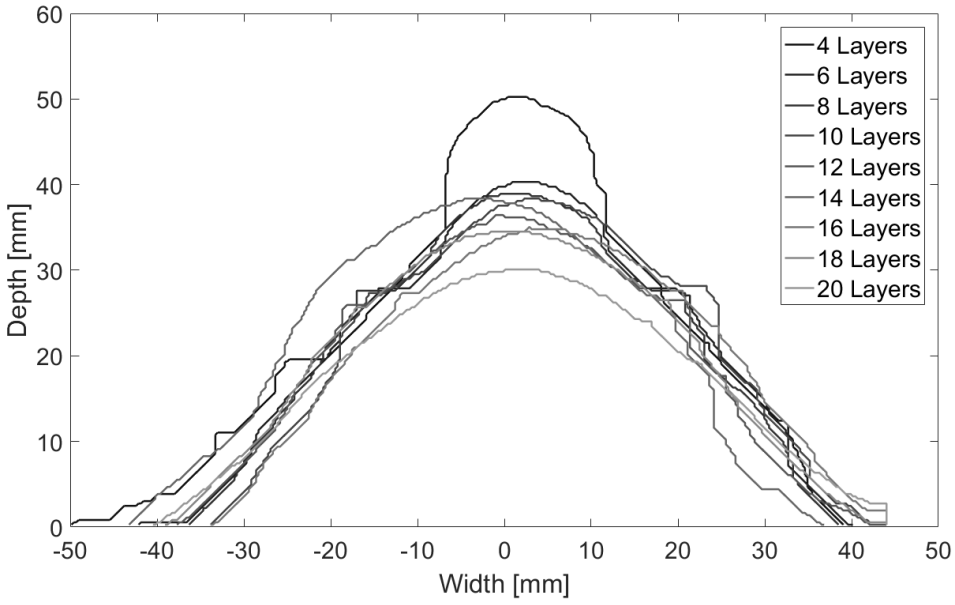

FIGURE 35. PLOT OF SHAPES FROM CONSTANT VELOCITY TESTING AT POINT OF MAXIMUM VOLUME.

The four-layer test exhibits unique behavior in that the projectile shape can be seen at the point of maximum depth. Between six and four layers, the sample is no longer able to keep the deformation fully spread out past the diameter of the projectile as the gel collapses back. Other than this exception, the deformation profiles at maximum volume are fairly similar to each other, perhaps suggesting the projectile energy is the main factor in the maximum volume of a deformation.

3.3 – Fabric Effects

To compare the deformation response between fabrics of different properties, testing was conducted with samples of similar areal densities, but different fabrics. Thick Kevlar® samples containing 5 and 10 layers (2335 and 4670 g/m^2 respectively), and the thin Kevlar® containing 20 and 40 layers (2440 and 4880 g/m^2 respectively) were tested. These samples were impacted

with steel ball bearings at relatively low impact energies. Table 5 shows the testing parameters for this group of tests.

TABLE 5. PARAMETERS FOR FABRIC COMPARISON TESTS.

	Baseline	**Comparison**
Fabric Type	thick	thin
Number of Fabric Layers	5, 10	20, 40
Total Areal Density	2335, 4670 g/m^2	2440, 4880 g/m^2
Projectile	ball bearing	ball bearing
Projectile Velocity	50-200 m/s	50-200 m/s
Backing Material	20% Gel	20% Gel

Figure 36 shows a comparison of the maximum depths between the 5 layer thick fabric samples and the 20 layer thin fabric samples, while Figure 37 shows a comparison of the maximum depths between the 10 layer thick fabric samples and the 40 layer thin fabric samples. In both of these graphs, the thin fabric tests are normalized to the thick (baseline) fabric sample areal densities for a better comparison.

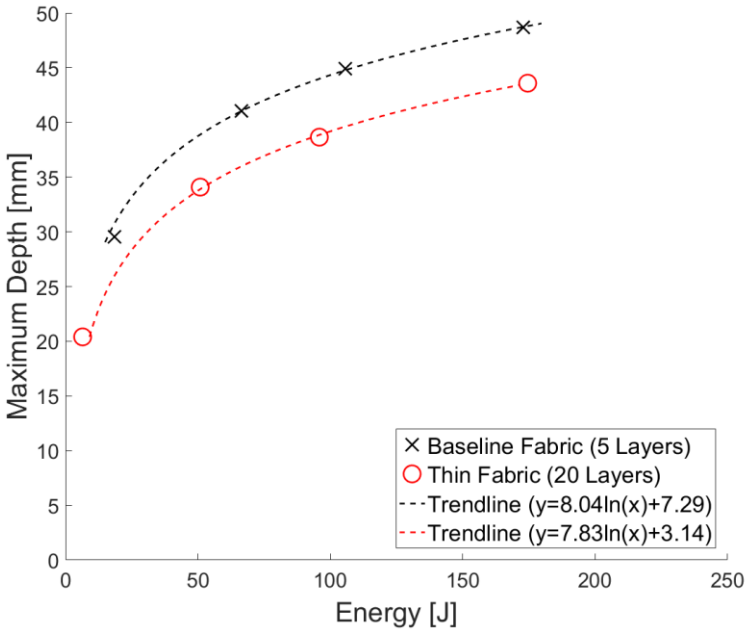

FIGURE 36. COMPARISON OF 5 LAYER THICK FABRIC SAMPLE AND 20 LAYER THIN FABRIC SAMPLE DEFORMATION DEPTH RESPONSE NORMALIZED TO BASELINE FABRIC TOTAL AREAL DENSITY.

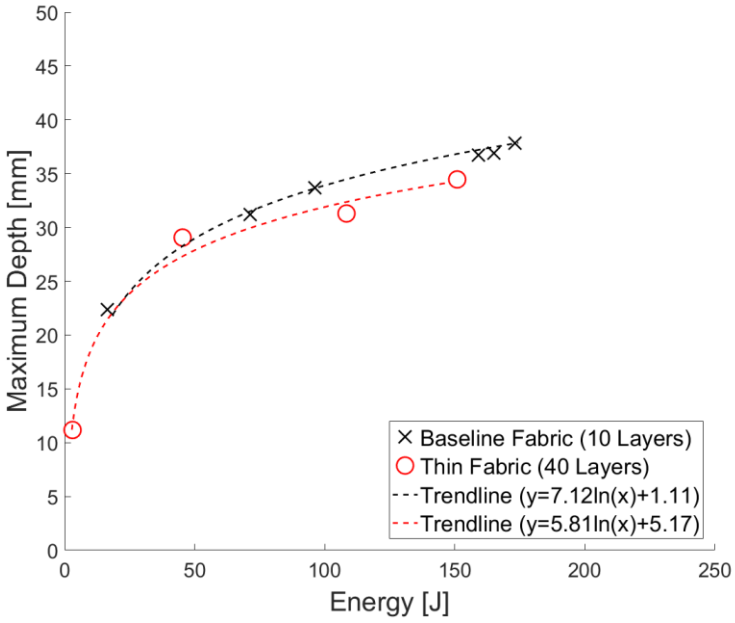

FIGURE 37. COMPARISON OF 10 LAYER THICK FABRIC SAMPLE AND 40 LAYER THIN FABRIC SAMPLE DEFORMATION DEPTH RESPONSE NORMALIZED TO BASELINE FABRIC TOTAL AREAL DENSITY.

Even with similar total areal densities, the deformation depths seen with the thin Kevlar® are less than with the thick Kevlar®. This is most likely due to the energy dissipation from friction between fabric layers, and the thin Kevlar® samples have approximately four times more layers for the same areal density. However, the thin fabric was also made of a slightly stiffer and stronger Kevlar® material, which could also explain the variation. Figure 38 shows a comparison of the maximum volumes between the 5 layer thick fabric samples and the 20 layer thin fabric samples, while Figure 39 shows a comparison of the maximum volumes between the 10 layer thick fabric samples and the 40 layer thin fabric samples.

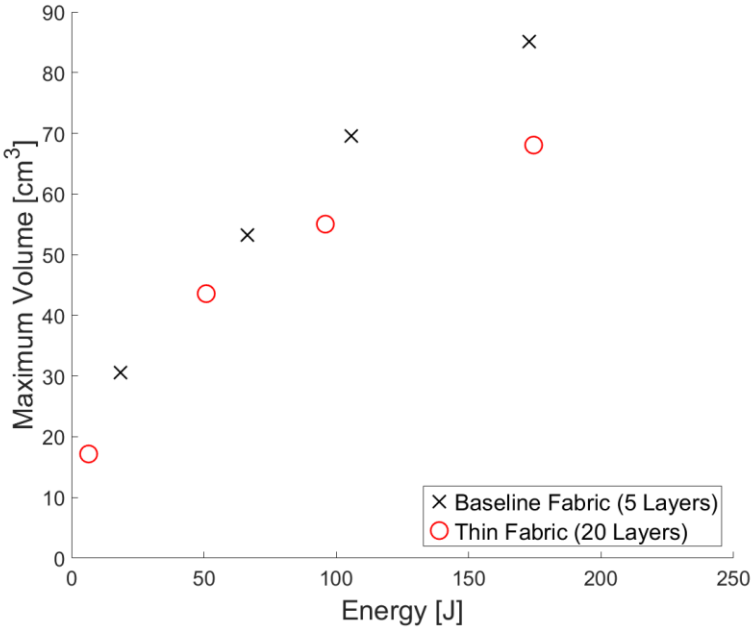

FIGURE 38. COMPARISON OF 5 LAYER THICK FABRIC SAMPLE AND 20 LAYER THIN FABRIC SAMPLE DEFORMATION VOLUME RESPONSE.

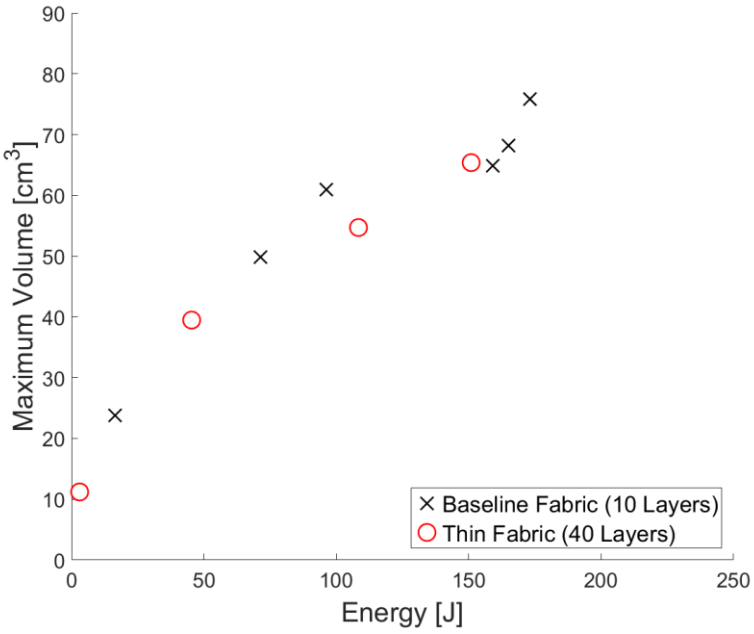

FIGURE 39. COMPARISON OF 10 LAYER THICK FABRIC SAMPLE AND 40 LAYER THIN FABRIC SAMPLE DEFORMATION VOLUME RESPONSE.

The thin fabric samples have slightly lower maximum deformation volumes than the thick fabric samples. This is another indicator that the thin fabric samples absorb more energy than the thick fabric samples for the same areal density. Figure 40 shows a comparison of the side profile shapes at maximum depth seen in the thick and thin fabric samples at a projectile velocity of 200 ± 9 m/s.

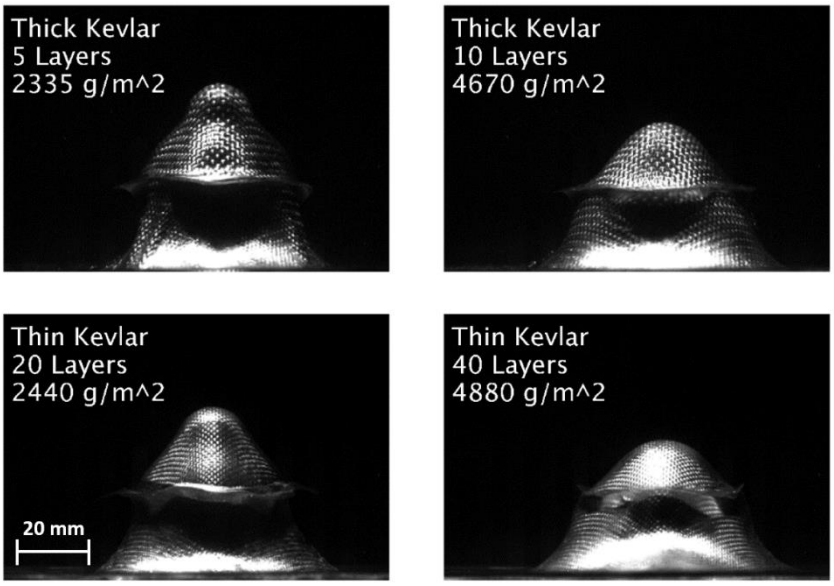

FIGURE 40. COMPARISON OF THICK AND THIN FABRIC SAMPLES WITH SIMILAR AREAL DENSITIES.

The deformation response in the thin Kevlar® samples is slightly wider and slightly shallower than the thick Kevlar®. This response would be considered better performance for a body armor as it reduces the impact on the wearer.

3.4 – Projectile Effects

To determine the effect of a deformable versus a non-deformable projectile would have, test were conducted with 15 layers of the thick Kevlar® fabric at various velocities with both 9mm FMJ and steel ball bearing projectiles. Parameters for this group of tests are given in Table 6.

TABLE 6. PARAMETERS FOR PROJECTILE COMPARISON TESTS.

	Baseline	Comparison
Fabric Type	thick	thick
Number of Fabric Layers	15	15
Total Areal Density	7005 g/m^2	7005 g/m^2
Projectile	ball bearing	9mm FMJ
Projectile Velocity	50-350 m/s	50-350 m/s
Backing Material	20% Gel	20% Gel

Figure 41 shows the ball bearing and the 9 mm FMJ projectiles before and after being shot at around 400 m/s, for a comparison of how they deform.

FIGURE 41. 9 MM FMJ (LEFT COLUMN) AND .50 CALIBER STEEL BALL BEARING (RIGHT COLUMN) BEFORE (TOP ROW) AND AFTER (BOTTOM ROW) IMPACTING THE TARGET.

The ball bearings do not deform in any measurable way from the impacts seen in this testing. The 9mm FMJ's, however, experience significant deformation, as can be seen in Figure 41.

Figure 42 shows how the maximum depths at different velocities change with the different projectiles.

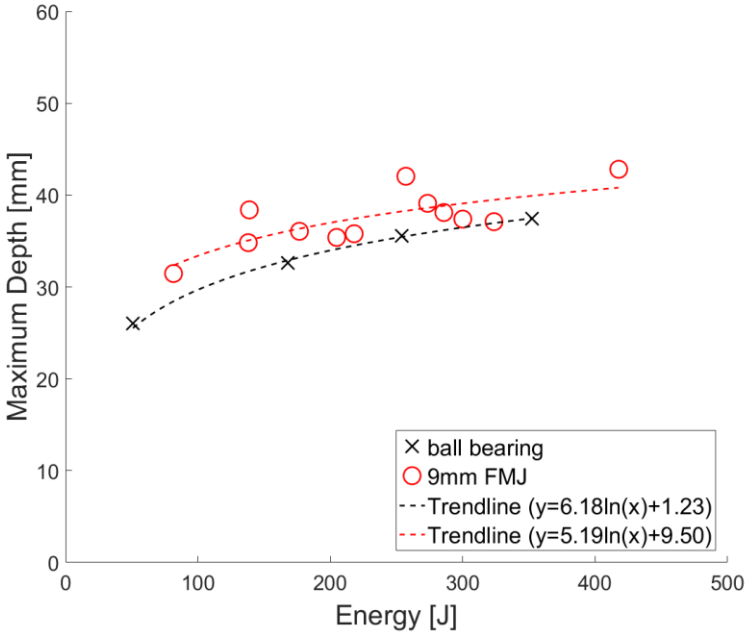

FIGURE 42. MAXIMUM DEFORMATION DEPTH COMPARISON FOR DIFFERENT PROJECTILES.

It can be seen that the deformation depths increase around 3 to 4 mm on average, when going from the ball bearing to the 9mm FMJ. Figure 43 shows how the maximum deformation volumes change between the two projectiles.

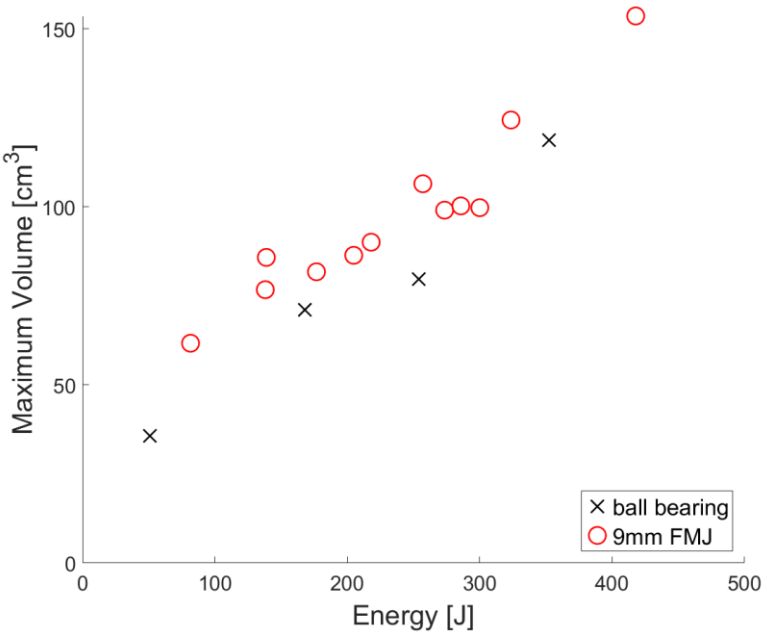

FIGURE 43. COMPARISON OF MAXIMUM DEFORMATION VOLUME FOR DIFFERENT PROJECTILES.

The maximum deformation volumes are slightly lower for the ball bearing versus the 9mm FMJ. This is most likely due to the deformable nature of the projectile pushing the deformation wider as it deforms on impact. In addition, more energy is being transferred through the fabric since the impact force is concentrated on a smaller area.

3.5 – Backing Material Effects

To determine the effect the backing material has on the deformation parameters, tests were conducted with 10 layers of the thick Kevlar® fabric at various velocities with both 10% and 20% ballistics gel backings. Parameters of this group of tests are given in Table 7.

TABLE 7. PARAMETERS FOR BACKING MATERIAL COMPARISON TESTS.

	Baseline	Comparison
Fabric Type	thick	thick
Number of Fabric Layers	10	10
Total Areal Density	4670 g/m^2	4670 g/m^2
Projectile	ball bearing	ball bearing
Projectile Velocity	50-300 m/s	50-300 m/s
Backing Material	20% Gel	10% Gel

Figure 44 shows how the maximum depths at different velocities change with the different backing materials.

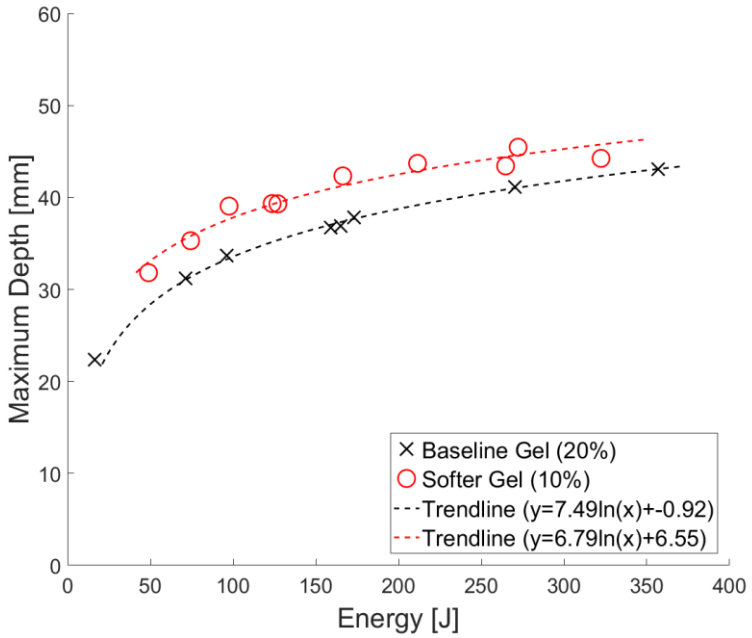

FIGURE 44. MAXIMUM DEFORMATION DEPTH COMPARISON FOR 10% AND 20% BALLISTICS GEL.

It can be seen that the deformation depths increase around 4 to 5 mm on average, when going from the 20% (stiffer) gel to the 10% (softer) gel. In addition, deformations in the 10% gel

took approximately 50% longer on average to reach maximum deformation than in the 20% gel. Figure 45 shows plots of the depth versus time history for a shot at 153 ± 1 m/s and 257 ± 1 m/s.

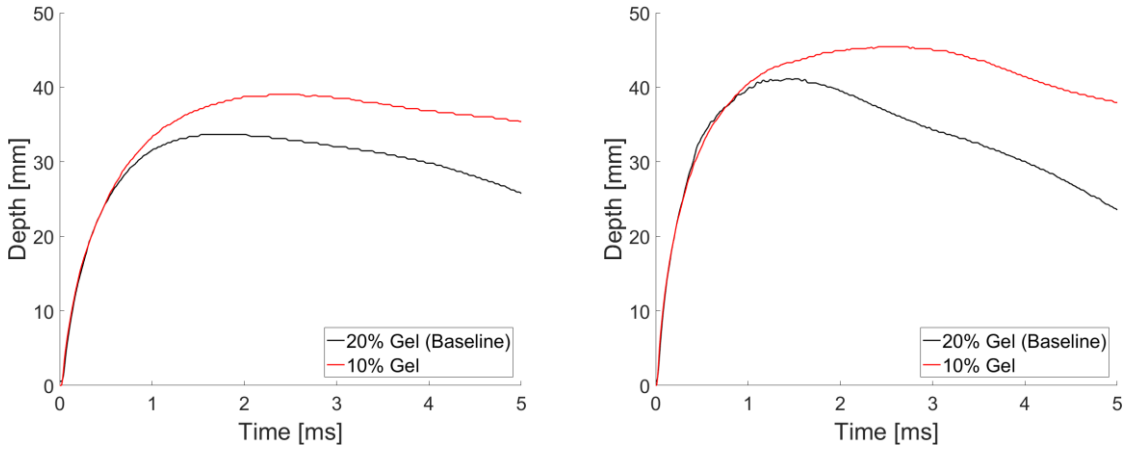

FIGURE 45. DEPTH VERSUS TIME COMPARISON BETWEEN 20% AND 10% GEL FOR SHOTS AT 153 ± 1 M/S (LEFT) AND 257 ± 1 M/S (RIGHT).

The deformation depths follow closely until near the point of maximum deformation. The viscoelastic nature of ballistics gel may explain this response. At the initial high loading rates, the gels appear to have the same stiffness but deviate near the point of maximum deformation. This suggests that the viscous properties are similar between the gels, and dominate at the initial loading rates, but the 20% gel has a higher rate of elastic recovery. This would also explain the difference in behavior seen after maximum deformation. Figure 46 shows how the maximum deformation volumes change between the two backing materials.

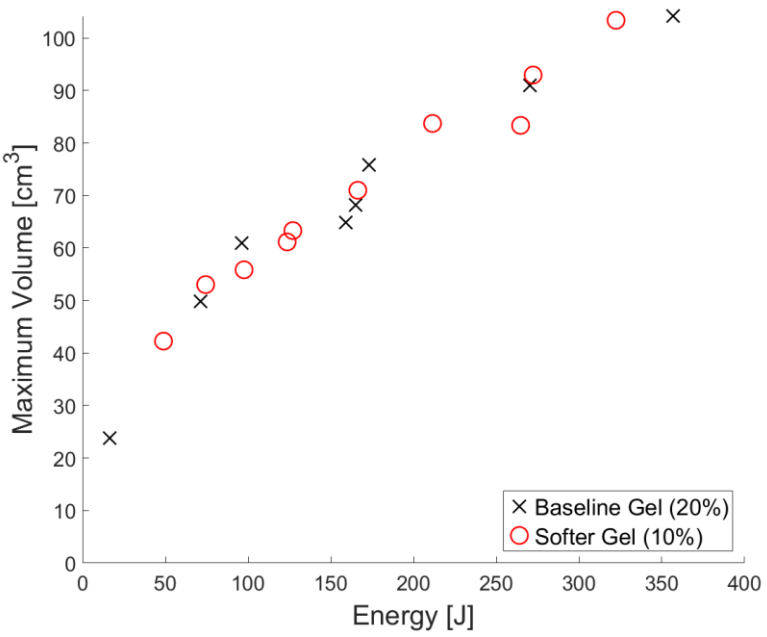

FIGURE 46. COMPARISON OF MAXIMUM DEFORMATION VOLUME FOR 10% AND 20% BALLISTICS GEL.

Interestingly, the maximum deformation volumes do not change significantly between the two ballistics gels in these tests. However, the shapes at these maximum volumes are vastly different. Figure 47 shows examples of the side profiles for two tests conducted at 203 ± 2 m/s (or around 170 J projectile energy) at their maximum volumes.

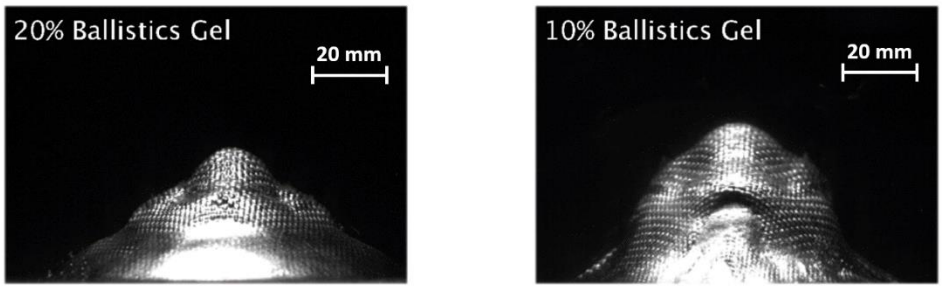

FIGURE 47. DIFFERENCE IN SHAPES AT MAXIMUM VOLUME FOR THE 20% AND 10% BALLISTICS GELS.

The maximum volume deformation shape for the 20% gel is wider and flatter than the 10% gel. This illustrates why it is extremely important to choose a backing material that approximates well the properties of human tissue, since the response changes so significantly.

3.6 – Conclusions

Data was obtained on the depths and shapes of back face deformations during impacts with different fabric and projectile parameters. Testing has shown that maximum depth increases with decreasing total areal density. In addition, when changing from a 467 g/m^2 Kevlar® K29 fabric to a 122 g/m^2 Kevlar® KM2Plus fabric, reduced maximum deformation depths were observed. This could be due to having more layer-to-layer friction available to dissipate energy, or the slightly increased stiffness and strength of the KM2Plus fabric. 9 mm FMJ projectiles produce slightly deeper deformation depths than the 12.7 mm steel ball bearings. This is most likely because of the smaller projectile contact area as the projectile impacts the armor, resulting in a higher amount of kinetic energy per cross-sectional area as the sample is loaded by the projectile. Lastly, the deformation response is shown to be highly dependent on the backing material properties, with 10% ballistics gel seeing 4 to 5 mm deeper deformations on average than 20% ballistics gel.

CHAPTER 4 – CONCLUSIONS AND FUTURE WORK

In this chapter, the major discoveries of this research are outlined, and future areas of exploration are suggested.

4.1 – Conclusions

An experimental setup has been developed that enables measuring the magnitude and rate of back face deformation of body armor samples during impact events. High-speed cameras are used to capture images of the deformation during impact, which are then converted to black and white to get desired data. With this setup and the processing method described in Chapter 2, the side profile of a deformation during impact can obtained, allowing many important parameters to be calculated such as depth, shape, and volume as a function of time. This enabled discovery of a transient ring that appears in back face deformations, resulting from air trapped between the sample and the backing material. In future work, data obtained from this method could be combined with medical information to accurately model injury in the body.

Data was obtained on the depths and shapes of back face deformations during impacts with different fabric and projectile parameters. Specifically:

1. Maximum volume of a deformation after projectile impact is attained significantly after maximum depth is achieved. This information has not been previously reported and could be significant when correlating displacement to injury.
2. Maximum depth decreases with increasing total areal density, as more material is available to absorb the impact energy.

3. When holding the total areal density of the sample constant, but changing from a 467 g/m^2 Kevlar® K29 fabric to a 122 g/m^2 Kevlar® KM2Plus fabric, reduced maximum deformation depths were observed. This could be due to having more layer-to-layer friction available to dissipate energy, or the slightly increased stiffness and strength of the KM2Plus fabric.
4. 9 mm FMJ projectiles produce slightly deeper deformation depths than the 12.7 mm steel ball bearings. This is most likely because of the greater amount of kinetic energy per cross-sectional area for the 9 mm FMJ projectiles as they impact the armor sample.
5. The backing material stiffness has a significant impact on the deformation response. When changing from 20% ballistics gelatin to 10% ballistics gelatin, the deformation depths observed in these tests increased 4-5 mm on average.

Overall, this work serves to show the influence of specific parameters discussed above on the impact performance of ballistic fabrics, as well as inform future directions of research in this area.

4.2 – Future Work

Several avenues of future work are recommended.

- Since the data in this work is based on a limited number of trials, it would be beneficial to conduct more exhaustive testing from a design of experiments approach to establish the statistical significance of the observations.

- When more data is obtained, scaling laws could be developed to predict armor performance based on the parameters and/or finite element models could be developed and validated for prediction of performance.
- Since there is concern of current clay backed testing's applicability to higher rate deformations seen in hard body armor, testing could be conducted with the setup described in this work on hard body armor to determine how much faster the deformations develop as well as determining trends in the shapes and volumes.

REFERENCES

[1] C. C. Yang, T. Ngo, and P. Tran, "Influences of weaving architectures on the impact resistance of multi-layer fabrics," *Mater. Des.*, vol. 85, 2015.

[2] C. Ha-Minh, A. Imad, F. Boussu, and T. Kanit, "On analytical modelling to predict of the ballistic impact behaviour of textile multi-layer woven fabric," *Compos. Struct.*, vol. 99, 2013.

[3] B. A. Cheeseman and T. A. Bogetti, "Ballistic impact into fabric and compliant composite laminates," *Compos. Struct.*, vol. 61, no. 1–2, pp. 161–173, 2003.

[4] A. Tabiei and G. Nilakantan, "Ballistic Impact of Dry Woven Fabric Composites: A Review," *Appl. Mech. Rev.*, vol. 61, no. 1, p. 10801, 2008.

[5] T. J. Singh and S. Samanta, "Characterization of Kevlar® Fiber and Its Composites: A Review," in *Materials Today: Proceedings*, 2015, vol. 2, no. 4–5.

[6] S. Sockalingam, S. C. Chowdhury, J. W. Gillespie, and M. Keefe, "Recent advances in modeling and experiments of Kevlar® ballistic fibrils, fibers, yarns and flexible woven textile fabrics - a review," *Text. Res. J.*, vol. 0, no. 0, 2016.

[7] R. Jack, J. R. Vinson, and J. William, "Modeling ballistic impact into flexible materials," *AIAA J.*, vol. 28, no. 12, pp. 2098–2103, 1990.

[8] J. W. S. Hearle, C. M. Leech, A. Adeyefa, and C. R. Cork, "Ballistic impact resistance of multi-layer textile fabrics," pp. 1–244, 1981.

[9] M. Mamivand and G. H. Liaghat, "A model for ballistic impact on multi-layer fabric targets," *Int. J. Impact Eng.*, vol. 37, no. 7, 2010.

[10] Y. Zhou, X. Chen, and G. Wells, "Influence of yarn gripping on the ballistic performance of woven fabrics from ultra-high molecular weight polyethylene fibre," *Compos. Part B Eng.*, vol. 62, 2014.

[11] Y. Zhou and X. Chen, "A numerical investigation into the influence of fabric construction on ballistic performance," *Compos. Part B Eng.*, vol. 76, pp. 209–217, Jul. 2015.

[12] X. Chen, Y. Zhou, and G. Wells, "Numerical and experimental investigations into ballistic performance of hybrid fabric panels," *Compos. Part B Eng.*, vol. 58, pp. 35–42, Mar. 2014.

[13] D. Zhang, Y. Sun, L. Chen, S. Zhang, and N. Pan, "Influence of fabric structure and thickness on the ballistic impact behavior of Ultrahigh molecular weight polyethylene composite laminate," *Mater. Des.*, vol. 54, 2014.

[14] X. Chen, F. Zhu, and G. Wells, "An analytical model for ballistic impact on textile based

body armour," *Compos. Part B Eng.*, vol. 45, no. 1, pp. 1508–1514, Feb. 2013.

[15] G. Nilakantan, R. L. Merrill, M. Keefe, J. W. Gillespie, and E. D. Wetzel, "Experimental investigation of the role of frictional yarn pull-out and windowing on the probabilistic impact response of Kevlar® fabrics," *Compos. Part B Eng.*, vol. 68, 2015.

[16] M. P. Rao, Y. Duan, M. Keefe, B. M. Powers, and T. A. Bogetti, "Modeling the effects of yarn material properties and friction on the ballistic impact of a plain-weave fabric," *Compos. Struct.*, vol. 89, no. 4, pp. 556–566, Aug. 2009.

[17] C. R. Cork and P. W. Foster, "The ballistic performance of narrow fabrics," *Int. J. Impact Eng.*, vol. 34, no. 3, pp. 495–508, Mar. 2007.

[18] I. S. Chocron-Benloulo, J. Rodriguez, and A. Sanchez-Galvez, "A simple analytical model to simulate textile fabric ballistic impact behavior," *Text. Res. J.*, vol. 67, no. 7, pp. 520–528, 1997.

[19] P. K. Porwal and S. L. Phoenix, "Modeling system effects in ballistic impact into multi-layered fibrous materials for soft body armor," *Int. J. Fract.*, 2005.

[20] H. Fang, M. Gutowski, M. Disogra, and Q. Wang, "A numerical and experimental study of woven fabric material under ballistic impacts," *Adv. Eng. Softw.*, vol. 96, 2016.

[21] G. Nilakantan and S. Nutt, "Effects of clamping design on the ballistic impact response of soft body armor," *Compos. Struct.*, vol. 108, pp. 137–150, Feb. 2014.

[22] A. Carroll and C. Soderstrom, "A new nonpenetrating ballistic injury.," *Ann. Surg.*, 1978.

[23] E. Hanlon and P. Gillich, "Origin of the 44-mm Behind-Armor Blunt Trauma Standard," *Mil. Med.*, vol. 177, no. 3, 2012.

[24] L. Cannon, "Behind Armour Blunt Trauma - an emerging problem," *J. R. Army Med. Corps*, vol. 147, no. MARCH 2001, pp. 87–96, 2001.

[25] "United States National Institute of Justice Standard (NIJ) Standard 0101.06," 2008.

[26] Board on Army Science and Technology, *Testing of Body Armor Materials: Phase III*. 2012.

[27] N. Montanarelli, C. E. Hawkins, M. A. Goldfarb, and T. F. Ciurej, "Protective Garments for Public Officials." 1973.

[28] L. W. Metker, R. N. Prather, and E. M. Johnson, "A Method for Determining Backface Signatures of Soft Body Armors." 1975.

[29] V. R. Clare, J. H. Lewis, A. P. Mickiewicz, and L. M. Sturdivan, "Blunt Trauma Data Correlation." 1975.

[30] M. A. Goldfarb, T. F. Ciurej, M. A. Weinstein, and L. W. Metker, "A Method for Soft

Body Armor Evaluation: Medical Assessment.” 1975.

[31] R. N. Prather and L. W. Metker, “Ballistic Test Matrix for Kevlar® Material,” 1976.

[32] R. N. Prather, C. L. Swann, and C. E. Hawkins, “Backface Signatures of Soft Body Armors and the Associated Trauma Effects.” 1977.

[33] L. Metker, R. Prather, and P. Coon, “A Method of Soft Body Armor Evaluation: Cardiac Testing.,” 1978.

[34] C. Hernandez, M. F. Buchely, and A. Maranon, “Dynamic characterization of Roma Plastilina No. 1 from Drop Test and inverse analysis,” *Int. J. Mech. Sci.*, vol. 100, pp. 158–168, Sep. 2015.

[35] C. P. Salisbury and D. S. Cronin, “Mechanical Properties of Ballistic Gelatin at High Deformation Rates,” *Exp. Mech.*, vol. 49, no. 6, pp. 829–840, Dec. 2009.

[36] J. Kwon and G. Subhash, “Compressive strain rate sensitivity of ballistic gelatin,” *J. Biomech.*, vol. 43, no. 3, pp. 420–425, Feb. 2010.

[37] M. Vollmer and K.-P. Mollmann, “High speed and slow motion: the technology of modern high speed cameras,” *Phys. Educ.*, vol. 46, no. 2, pp. 191–202, Mar. 2011.

[38] J. C. Roberts *et al.*, “Computational and experimental models of the human torso for non-penetrating ballistic impact.,” *J. Biomech.*, vol. 40, no. 1, pp. 125–36, Jan. 2007.

[39] L. Liu, Y. Fan, and W. Li, “Viscoelastic shock wave in ballistic gelatin behind soft body armor,” *J. Mech. Behav. Biomed. Mater.*, vol. 34, pp. 199–207, Jun. 2014.

[40] S. Luo, C. Xu, A. Chen, and X. Zhang, “Experimental investigation of the response of gelatine behind the soft body armor,” *Forensic Sci. Int.*, vol. 266, pp. 8–13, Sep. 2016.

[41] M. Karahan, A. Kuş, and R. Eren, “An investigation into ballistic performance and energy absorption capabilities of woven aramid fabrics,” *Int. J. Impact Eng.*, vol. 35, no. 6, pp. 499–510, Jun. 2008.

APPENDICES

Appendix A – Matlab Files for Processing Side View Image Data

```
% convertToBW.m

% Converts the grayscale images from high speed video and writes black &
% white frames to a .mat file to be used later. Also writes a check video
% to assess the qualtiy of the conversion

%Input and output file paths
grayFile = 'side.avi'; %path to grayscale high speed video (input)
bwMatFile = 'bwMat.mat'; %path to black and white array (output)
checkVidFile = 'checkVid1.mp4'; %path to check video file (output)

%Image conversion parameters
diskSize = 15; %Increase value to fill bigger gaps in the deformation area
deleteSize = 20; %Increase value to delete bigger artifacts in image
thresh = 10/255; %Increasing value converts less pixels to white
cutOverhangs = 1; %Option to eliminate(1) overhangs in profile or not(0)

%Calibration parameters
oneDepth = 166.5; %Depth location of 1 inch calibration rod (pixels)
halfDepth = 212.5; %Depth location of 0.5 inch calibration rod (pixels)
gelSurf = 1.4; %gel offset depth from metal surface (millimeters)

%%%%%%%%%%%%%%%%%%%%%%%%%%%%%%%%%%%%%%%%%%%%%%%%%%%%%%%%%%%%%%%%%%%%%%%%%%%

%Initialize check video
checkVid = VideoWriter(checkVidFile, 'MPEG-4');
checkVid.Quality =100;
checkVid.FrameRate = 20;
open(checkVid)

v = VideoReader(grayFile);
cal = abs((halfDepth-oneDepth)/0.5/25.4); %pixels/mm
res = size(read(v,1)); %resolution of input video
botCrop = round((2*halfDepth-oneDepth)-cal*gelSurf,0); %zero location (px)
if botCrop < res(1)
    res(1) = botCrop; %crops frame to zero location
else
    display('Check calibration values, may not be valid')
end

bwMat = zeros(res(1),res(2),v.NumberOfFrames,'logical');

for i = 1:v.NumberOfFrames

    %This block reads frame, converts to black & white and stores in bwMat
    raw = read(v,i);
    raw = raw(1:res(1),:); %crops bottom to zero location
    bw = imbinarize(raw,thresh);
    bw = bwareaopen(bw,deleteSize);
    se = strel('disk',diskSize);
    bw = imclose(bw,se);
```

```
    bw = imfill(bw,'holes');

    %This block cuts overhangs if option is set
    if cutOverhangs
        for a = 1:res(2)
            for b = res(1):-1:1
                if not(bw(b,a))
                    bw(1:b,a) = zeros(1,b);
                    break
                end
            end
        end
    end

    bwMat(:,:,i) = bw; %stores frame

    %This block writes select frames to the check video
    if i <250 && not(mod(i,2))
        frame = uint8(255 * bw);
        frame = cat(2,frame,raw*3);
        writeVideo(checkVid,frame);
    end
end
save(bwMatFile, 'bwMat');
close(checkVid)
```

```
% writeData.m

% Takes the matrix of black & white frames output from convertToBW.m and
% calculates the deformation depth, width (at a certain depth), projected
% area, and volume, and writes it to a csv file.

%Input and output file paths
bwMatFile = 'bwMat.mat'; %path to black and white data matrix (input)
outputFile = 'data.csv'; %path to data file (output)
checkFigFile = 'checkFig.fig'; %path to check figure file (output)

%Video properties for setting time vector
camFrameRate = 100000; %fps
zeroFrame = 11; %frame where deformation begins

%Calibration parameters
oneDepth = 166.5; %Depth location of 1 inch calibration rod (pixels)
halfDepth = 212.5; %Depth location of 0.5 inch calibration rod (pixels)

%Code will write the width of deformation at a certain depth
widthDepth = 5; %mm

%%%%%%%%%%%%%%%%%%%%%%%%%%%%%%%%%%%%%%%%%%%%%%%%%%%%%%%%%%%%%%%%%%%%%%%%%%%

%Initialize variables that will be needed
cal = (halfDepth-oneDepth)/0.5/25.4; %px/mm
load(bwMatFile);
s = size(bwMat);
widDep = round(s(1)-widthDepth*cal,0); %pixel location
t = ((1:s(3))'-(zeroFrame))/camFrameRate*1000; %ms

%Initialize vectors for storing data
Depth = zeros(s(3),1);
Area = zeros(s(3),1);
Vol = zeros(s(3),1);
Wid = zeros(s(3),1);

for i = 1:s(3)
    bw = bwMat(:,:,i);
    [row,col]=find(bw); %determines locations of white pixels

    %Find depth location in px
    if isempty(row)==1
        Depth(i)=s(1);
    else
        Depth(i)=min(row);
    end

    %Find area in px^2
    Area(i)=length(row);

    %Find volume in px^3
    if isempty(col)==1
```

```
        Vol(i) = 0;
    else
        Vol(i) = findVolume(col);
    end

    %Finds width of deformation at specified depth
    Wid(i) = length(find(bw(widDep-1:widDep+1,:)))/3; %pixels
end

%Convert from pixels to physical units
Depth = (s(1)-Depth)/cal; %mm
Wid = Wid/cal; %mm
Area = Area/cal^2/(10^2); %cm^2
Vol = Vol/cal^3/(10^3); %cm^3

%Get data ready to write to file
dat = cat(2,t,Depth,Wid,Area,Vol);

%Write header and data to file
fid = fopen(outputFile, 'w');
fprintf(fid, ...
    'Time [s], Depth [mm], Width [mm], Area [cm^2], Volume [cm^3]\n');
fclose(fid);
dlmwrite(outputFile, dat, '-append', 'delimiter', ',');

%Make plot to check results and save
figure(1)
plot(t,dat(:,2:5))
l1 = legend({'Depth [mm]', 'Width [mm]', 'Area [cm^2]', 'Volume [cm^3]'});
xlabel('time [ms]')
ylabel('See legend for units')
savefig(gcf,checkFigFile)
```

```
function [ volume ] = findVolume( X )
% Finds the volume of a deformation by revolving each side
% of the deformation then averaging. Output value is in units
% of cubic pixels

cent = mean(X); %each pixel location has the same area

%initialize variables to accumulate volumes
left = 0;
right = 0;

for i = 1:length(X)
    %Accumulate volumes of the left rings
    if X(i) < cent
        left = left + pi*((cent-X(i)+0.5)^2-(cent-X(i)-0.5)^2);
    %Accumulate volumes of the right rings
    else
        right = right + pi*((cent-X(i)+0.5)^2-(cent-X(i)-0.5)^2);
    end
end
%Average volumes from left and right sides
volume = (abs(right)+abs(left))/2;
end
```

Appendix B – Table of data for all shots

Test ID	Projectile	Fabric Type	Velocity [m/s]	Num Layers	Energy [J]	Max Depth [mm]	Time to Max Depth [ms]	Max Volume [cm^3]	Time to Max Volume [ms]
Thick5-50_1	ball b.	thick	67.0	5	18.5	29.54	1.78	30.57	4.05
Thick5-100_1	ball b.	thick	127.0	5	66.4	41.05	1.82	53.24	4.29
Thick5-150_1	ball b.	thick	160.2	5	105.6	44.91	1.62	69.55	3.98
Thick5-200_1	ball b.	thick	204.8	5	172.8	48.68	1.57	85.11	4.09
Thick5-250_1	ball b.	thick	247.2	5	251.8	52.18	1.61	113.92	3.88
Thick5-300_1	ball b.	thick	304.7	5	382.5	54.94	1.14	117.26	4.28
Thick10-50_1	ball b.	thick	63.2	10	16.4	22.36	1.76	23.80	3.87
Thick10-100_1	ball b.	thick	131.6	10	71.3	31.20	1.59	49.84	3.54
Thick10-150_1	ball b.	thick	152.8	10	96.2	33.68	1.53	60.95	4.03
Thick10-200_2	ball b.	thick	196.5	10	159.1	36.72	1.80	64.87	3.84
Thick10-200_3	ball b.	thick	200.2	10	165.0	36.90	1.63	68.19	3.73
Thick10-200_1	ball b.	thick	205.0	10	173.1	37.82	1.35	75.83	4.02
Thick10-250_1	ball b.	thick	256.2	10	270.3	41.14	1.41	90.97	3.58
Thick10-300_1	ball b.	thick	294.3	10	356.8	43.07	1.29	104.19	4.76
Thick15-25_1	ball b.	thick	19.4	15	1.5	7.84	1.88	6.53	2.47
Thick15-100_1	ball b.	thick	111.2	15	50.9	26.02	1.98	35.70	3.35
Thick15-200_1	ball b.	thick	201.9	15	167.9	32.62	1.61	71.09	3.65
Thick15-250_1	ball b.	thick	248.3	15	253.9	35.56	1.49	79.71	3.33
Thick15-300_1	ball b.	thick	292.5	15	352.3	37.43	1.34	118.71	4.70
Thick20-150_1	ball b.	thick	158.0	20	102.8	30.46	2.83	57.29	3.74
Thick20-250_2	ball b.	thick	249.3	20	255.9	35.34	2.14	86.20	3.57
Thick20-350_1	ball b.	thick	349.8	20	504.0	40.37	1.45	162.79	3.80
Thick25-350_2	ball b.	thick	349.7	25	503.6	41.69	1.69	115.42	4.29
ConsV-4_1	ball b.	thick	196.4	4	159.0	54.48	1.98	98.59	3.63
ConsV-6_1	ball b.	thick	203.7	6	170.9	45.37	1.66	81.44	3.53
ConsV-8_1	ball b.	thick	202.9	8	169.6	42.52	1.66	75.94	3.70
ConsV-10_1	ball b.	thick	199.7	10	164.2	40.49	1.74	76.46	3.59
ConsV-12_1	ball b.	thick	194.0	12	155.1	37.64	1.73	74.35	3.68
ConsV-14_1	ball b.	thick	203.2	14	170.1	38.38	2.28	80.02	3.57
ConsV-16_1	ball b.	thick	199.1	16	163.2	35.43	2.56	72.86	3.62
ConsV-18_1	ball b.	thick	198.9	18	163.0	34.79	2.91	75.73	3.53
ConsV-20_1	ball b.	thick	195.0	20	156.6	30.55	1.66	69.88	3.36
Thin20-50_1	ball b.	thin	39.7	20	6.5	19.52	1.83	16.43	3.08
Thin20-100_1	ball b.	thin	111.1	20	50.9	32.62	1.50	41.70	3.70
Thin20-150_1	ball b.	thin	152.6	20	95.9	36.99	1.51	52.67	3.67
Thin20-200_1	ball b.	thin	205.8	20	174.5	41.71	1.26	65.13	3.73
Thin40-50_1	ball b.	thin	27.4	40	3.1	10.70	1.68	10.72	2.59
Thin40-100_1	ball b.	thin	105.0	40	45.4	27.81	1.86	37.78	3.92
Thin40-150_1	ball b.	thin	162.2	40	108.4	29.95	1.32	52.35	3.51
Thin40-200_1	ball b.	thin	191.4	40	150.9	32.98	1.53	62.57	3.43
Thick15-9mm_100_1	9mm	thick	136.6	15	81.6	31.46	2.22	61.70	3.78
Thick15-9mm_175_1	9mm	thick	177.6	15	138.0	34.82	2.32	76.73	3.62
Thick15-9mm_150_1	9mm	thick	178.1	15	138.8	38.39	2.56	85.79	3.72
Thick15-9mm_200_2	9mm	thick	200.9	15	176.7	36.06	2.55	81.76	3.64
Thick15-9mm_225_1	9mm	thick	216.4	15	204.8	35.39	1.86	86.38	3.52
Thick15-9mm_200_1	9mm	thick	223.2	15	218.0	35.79	1.62	90.07	3.44
Thick15-9mm_250_2	9mm	thick	242.4	15	257.0	42.05	2.73	106.47	3.47
Thick15-9mm_250_3	9mm	thick	250.0	15	273.5	39.10	1.95	99.06	3.62
Thick15-9mm_250_1	9mm	thick	255.5	15	285.7	38.10	1.56	100.25	3.28
Thick15-9mm_275_2	9mm	thick	261.9	15	300.0	37.39	1.46	99.76	3.37
Thick15-9mm_300_2	9mm	thick	271.9	15	323.6	37.10	1.48	124.37	3.17
Thick15-9mm_325_1	9mm	thick	309.0	15	417.8	42.81	1.68	153.57	3.07
Thick10_10perc_50_1	ball b.	thick	109.0	10	48.9	31.82	2.61	42.27	4.43
Thick10_10perc_100_1	ball b.	thick	134.4	10	74.4	35.29	2.31	53.03	4.10
Thick10_10perc_150_2	ball b.	thick	153.9	10	97.6	39.06	2.27	55.85	3.90
Thick10_10perc_175_1	ball b.	thick	173.3	10	123.6	39.33	2.31	61.16	3.59
Thick10_10perc_150_1	ball b.	thick	175.7	10	127.1	39.30	2.68	63.32	4.40
Thick10_10perc_200_2	ball b.	thick	200.9	10	166.3	42.33	2.31	71.00	4.10
Thick10_10perc_225_1	ball b.	thick	226.6	10	211.5	43.70	2.35	83.73	3.90
Thick10_10perc_250_2	ball b.	thick	253.5	10	264.7	43.43	2.06	83.36	3.29
Thick10_10perc_250_1	ball b.	thick	257.1	10	272.2	45.45	2.41	92.95	3.72
Thick10_10perc_275_1	ball b.	thick	279.7	10	322.3	44.25	2.14	103.38	5.89